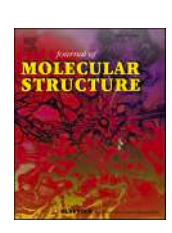
ELSEVIER

Contents lists available at ScienceDirect

Journal of Molecular Structure

journal homepage: www.elsevier.com/locate/molstr



Exploring Pyrazole integrated thiazole molecular hybrids for antitubercular activity: Synthesis, spectral characterization, DFT, ADME, and docking studies

Yuvraj R. Sable ^a, Vishnu A. Adole ^{a,*} ^o, Rahul A. Shinde ^{b,*} ^o, Hemant S. Deshmukh ^a, R. Rajesh ^c, Tahani Mazyad Almutairi ^d, Mahboob Alam ^e ^o, Mohammad Shahidul Islam ^{d,*} ^o

ARTICLE INFO

Keywords: Pyrazole Thiazole Tuberculosis Density functional theory Molecular docking Pharmacokinetics

ABSTRACT

A series of pyrazole-thiazole hybrid compounds (6a-6j) was synthesized and characterized to evaluate their potential as antitubercular agents. The synthetic strategy involved the nucleophilic substitution of chloro by morpholine in 5-chloro-3-methyl-1-phenyl-1H-pyrazole-4-carbaldehyde, followed by condensation with thiosemicarbazide and subsequent cyclization with aryl bromoketones. Structural confirmation of the synthesized compounds was achieved through FT-IR, ¹H NMR, and ¹³C NMR spectroscopy. The high-resolution mass spectrometry (HRMS) data of compounds 6a-6j confirmed their molecular formula and successful synthesis. kKey spectral features, including characteristic azomethine (-CH=N-) and thiazole ring absorption bands, confirmed the successful formation of the target compounds. Biological evaluation against Mycobacterium tuberculosis H37Rv revealed significant antitubercular activity, with compound 6i exhibiting the most potent inhibitory effect (MIC: 12.5 µg/mL), likely due to the electron-withdrawing trifluoromethyl group on the phenyl ring. Molecular docking studies targeting Cytochrome P450 14α -sterol demethylase (CYP51) indicated that compound 6i forms stable interactions, including hydrogen bonding with His101 and π -stacking with Phe399, resulting in a strong binding affinity (-8.9 kcal/mol). These interactions enhance its binding affinity, suggesting a potential mechanism of CYP51 inhibition. Additionally, a DFT study was conducted to gain deeper insights into the structural, chemical, spectroscopic, and electronic properties of compound 6i. The analysis revealed its stability and reactivity, supporting its molecular framework for further optimization. ADME studies confirmed that 6i possesses favorable pharmacokinetic and drug-like properties, suggesting it as a promising scaffold for the development of new antitubercular agents.

1. Introduction

Tuberculosis (TB) remains a major global health challenge, intensified by the rise of multidrug-resistant (MDR) and extensively drug-resistant (XDR) strains, underscoring the urgent need for novel antitubercular agents [1–3]. Current TB treatments require prolonged

multidrug regimens with severe side effects, reducing patient compliance and hindering global control efforts [4,5]. Identifying new molecular scaffolds with better efficacy, lower toxicity, and favorable pharmacokinetics is vital to improve outcomes and combat drug resistance in TB therapy. Heterocyclic scaffolds have garnered significant attention in medicinal chemistry due to their versatile biological

E-mail addresses: sabley70@gmail.com (Y.R. Sable), vishnuadole86@gmail.com (V.A. Adole), rahulshinde843@gmail.com (R.A. Shinde), Hemd144@gmail.com (H.S. Deshmukh), rajeshharini2210@gmail.com (R. Rajesh), talmutari1@ksu.edu.sa (T.M. Almutairi), mahboobchem@gmail.com (M. Alam), mislam@ksu.edu.sa (M.S. Islam).

https://doi.org/10.1016/j.molstruc.2025.142891

Received 13 February 2025; Received in revised form 1 June 2025; Accepted 3 June 2025 Available online 4 June 2025

0022-2860/© 2025 Elsevier B.V. All rights are reserved, including those for text and data mining, AI training, and similar technologies.

^a Research Centre in Chemistry, Mahatma Gandhi Vidyamandir's Loknete Vyankatrao Hiray Arts, Science and Commerce College, Panchavati, Nashik 422003, Maharashtra, (Affiliated to Savitribai Phule Pune University, Pune), India

^b Department of Chemistry, Mahatma Gandhi Vidyamandir's Maharaja Sayajirao Gaikwad Arts, Science and Commerce College, Malegaon, Nashik 423105, (Affiliated to Savitribai Phule Pune University, Pune), India

^c Department of Physics, Vel Tech High Tech Dr. Rangarajan Dr. Sakunthala Engineering College (Autonomous), Chennai, India

d Department of Chemistry, College of Science, King Saud University, P.O. Box 2455, Riyadh 11451, Saudi Arabia

^e Division of Chemistry and Biotechnology, Dongguk University, 123, Dongdaero, Gyeongjusi 780714, Republic of Korea

^{*} Corresponding authors.

Fig. 1. Literature reported biologically active pyrazole and thiazole compounds and well-known synthetic drugs.

activities [6-8]. Among these, thiazole, pyrazole, and morpholine moieties have been extensively investigated for their pharmacological potential. Thiazole derivatives, in particular, exhibit a broad spectrum of biological activities, including antimicrobial [9–11], anticancer [12,13], antiviral [14,15], antidiabetic [16], antimalarial anti-inflammatory [18], analgesic [19], antioxidant [20], and anticonvulsant [21] properties. Pyrazole-based compounds have been researched to exhibit significant biological activities, including antibacterial, anticancer, anti-Alzheimer antifungal, anti-inflammatory, and antioxidant effects [22-28]. Fig. 1 illustrates literature-reported biologically active pyrazole and thiazole compounds along with well-known synthetic drugs [29-32].

K. Veena et al. designed and synthesized a series of benzimidazole-linked thiazole derivatives, which were tested for activity against the *M. tuberculosis* H37Rv strain and two MDR-resistant clinical isolates [33]. Additionally, Lakshmi et al. developed a library of novel acetylene-containing 2-(2-hydrazinyl)thiazole derivatives, designed based on their physicochemical properties, and evaluated their potency against the *M. tuberculosis* H37Rv strain [34]. Recently, Marwa M. et al. evaluated a series of 3-(p-chlorophenyl)-1-phenylpyrazole derivatives for their antimicrobial activity against M. tuberculosis H37Rv and assessed their potential as InhA inhibitors [35]. Morpholine, a crucial pharmacophore in many bioactive molecules, enhances the lipophilicity and metabolic stability of drug candidates [36].

In this study, in continuation of our work on synthesises of bioactive thiazoles [37–40], we focus on the design and synthesis of new thiazole hybrids incorporating pyrazole and morpholine frameworks, aiming to evaluate their antitubercular potential. The rationale behind this hybridization approach is to integrate the beneficial pharmacological attributes of each moiety, thereby enhancing biological activity. To gain

insights into their biological activity, we have conducted density functional theory (DFT) calculations, absorption, distribution, metabolism, and excretion (ADME) studies, as well as molecular docking simulations. These computational and theoretical studies provide a comprehensive understanding of the structural, electronic, and pharmacokinetic properties of the synthesized hybrids, offering a rational basis for the synthesis of bioactive agents [41,42]. Molecular docking studies helps to identify the binding affinity and interactions of these molecules with key biological targets, which is essential for evaluating their therapeutic potential [43].

2. Materials and methods

2.1. General remarks

All reagents and solvents used in the synthesis were of analytical grade and were procured from commercially available sources. The reactions were monitored using thin-layer chromatography (TLC) on silica gel plates, and spots were visualized under UV light. The melting points of the synthesized compounds were determined in open capillary tubes and are uncorrected. The purity of the compounds was confirmed by TLC and further characterized using spectroscopic techniques such as FT-IR, 1 H NMR, 13 C NMR and HRMS methods. FT-IR spectra were recorded on an Agilent FT-IR spectrometer. NMR spectra were recorded on a Bruker spectrometer at 500 MHz for 1 H NMR and 126 MHz for 13 C NMR, using DMSO- d_6 as solvent with tetramethylsilane as an internal standard. Chemical shifts (δ) are given in parts per million (ppm) and coupling constants (J) are reported in Hertz (Hz).

$$H_3C$$
 H_3C
 H_3C

Scheme 1. Synthesis of intermediate 3 and pyrazole and morpholine integrated thiazole hybrids (6a-6j).

2.2. Experimental procedure for the synthesis of 3-methyl-5-morpholino-1-phenyl-1H-pyrazole-4-carbaldehyde

The compound 5-chloro-3-methyl-1-phenyl-1H-pyrazole-4-carbaldehyde (1) was previously synthesized [38]. A mixture of 5-chloro-3-methyl-1-phenyl-1H-pyrazole-4-carbaldehyde (1, 11.03 g, 0.05 mol), morpholine (2, 5.23 g, 0.006 mol), and potassium carbonate (10.36 g, 0.075 mol) was stirred in dry DMF at room temperature for 6 h. The reaction mixture was then poured into ice-cold water, and the precipitate formed was filtered, washed with water, and recrystallized from ethanol to afford 3-methyl-5-morpholino-1-phenyl-1H-pyrazole-4-carbaldehyde (3).

2.3. Experimental procedure for the synthesis of pyrazole-thiazole derivatives (6a-6j)

A solution of compound 3 (0.54 g, 0.002 mol) and thiosemicarbazide (4, 0.182 g, 0.002 mol) was prepared by dissolving them in 10 mL of ethanol. To this mixture, 2–3 drops of acetic acid were added as a catalyst, and the reaction was refluxed in an oil bath for 1 hour to facilitate the condensation process. Following this, the calculated quantity of aryl bromoketone (5a–5j, 0.002 mol) was gradually introduced into the reaction mixture, leading to the formation of a precipitate corresponding to the final product. The reaction progress was monitored by thin-layer chromatography (TLC). Upon completion, the reaction mixture was allowed to cool to room temperature, and the resulting solid was collected by filtration. The crude product was then thoroughly washed with cold ethanol to remove any impurities, affording the final compounds 6a–6j in pure form. The detailed synthetic sequence is given in Scheme 1 and the physicochemical data in Table 1.

2.4. Spectral data

$2.4.1. \ \ 3\text{-methyl-5-morpholino-1-phenyl-1H-pyrazole-4-carbal dehyde} \ \ (3)$

 1 H NMR (500 MHz, DMSO- d_{6}) δ 9.95 (s, 1H, CHO), 7.61 – 7.58 (m, 2H, Ar-H), 7.56 – 7.52 (m, 2H, Ar-H), 7.46 – 7.42 (m, 1H, Ar-H), 3.58 – 3.54 (m, 4H, O(CH₂)₂), 3.11 – 3.07 (m, 4H, N(CH₂)₂), 2.36 (s, 3H, CH₃); 13 C NMR (126 MHz, DMSO- d_{6}) δ 183.80 (CHO—C), 152.03 (Ar-C), 150.48 (Ar-C), 138.74 (Ar-C), 129.09 (Ar-C), 128.05 (Ar-C), 124.69 (Ar-C)

C), 111.94 (Ar-C), 65.87 (O(CH₂)₂), 50.37 (N(CH₂)₂), 13.65 (CH₃)

2.4.2. (E)-4-(3-methyl-1-phenyl-4-((2-(4-phenylthiazol-2-yl) hydrazineylidene)methyl)-1H-pyrazol-5-yl)morpholine (6a)

FT-IR (ν , cm⁻¹): 3367 (NH), 3041 (Ar-CH), 2829 (sp^3 -CH), 1622 (C=N), 1605 (C=C), 1544 (C=C), 1499 (C=C), 1329 (C–N), 1260 (C–O–C), 1191 (C–N); ¹H NMR (500 MHz, DMSO- d_6) δ 11.88 (s, 1H, NH), 8.30 (s, 1H, imine H), 7.85 (d, J=7.4 Hz, 2H, Ar-H), 7.62 (d, J=7.4 Hz, 2H, Ar-H), 7.52 (t, J=7.8 Hz, 2H, Ar-H), 7.44 – 7.37 (m, 3H, Ar-H), 7.33 – 7.27 (m, 2H, Ar-H and Thiazole-H), 3.64 – 3.55 (m, 4H, O (CH₂)₂), 3.12 – 3.03 (m, 4H, N(CH₂)₂), 2.38 (s, 3H, CH₃); ¹³C NMR (126 MHz, DMSO- d_6) δ 168.87 (Thiazole-C2), 148.61 (Pyrazole-C5), 147.63 (Pyrazole-C3), 139.36 (Imine H), 137.20 (Thiazole-C4), 134.44 (Ar-C), 129.44 (Ar-C), 129.35 (Ar-C), 129.12 (Ar-C), 128.25 (Ar-C), 127.87 (Ar-C), 126.12 (Ar-C), 124.81 (Ar-C), 108.89 (Thiazole-C5), 103.82 (Pyrazole-C4), 66.79 (O(CH₂)₂), 50.82 (N(CH₂)₂), 15.31 (CH₃); HRMS (M+H)⁺: 445.1810 (calculated) and 445.1818 (observed) for C₂₄H₂₄N₆OS

2.4.3. (E)-4-(3-methyl-4-((2-(4-(naphthalen-2-yl)thiazol-2-yl) hydrazineylidene)methyl)-1-phenyl-1H-pyrazol-5-yl)morpholine (6b)

FT-IR (cm⁻¹): 3398 (NH), 3051 (Ar-CH), 2963 (sp^3 -CH), 2835 (sp^3 -CH), 1619 (C=N), 1542(C=C), 1451 (C=C), 1260 (C—O), 1174 (C—N); 1109 (C—C); ¹H NMR (500 MHz, DMSO- d_6) δ 11.97 (s, 1H, NH), 8.38 (s, 1H, imine H), 8.31 (s, 1H, Ar-H), 8.03 – 7.90 (m, 4H, Ar-H), 7.63 (d, J=7.6 Hz, 2H, Ar-H), 7.57 – 7.48 (m, 4H, Ar-H), 7.45 (s, 1H, Thiazole-H), 7.40 (t, J=7.4 Hz, 1H, Ar-H), 3.67 – 3.56 (m, 4H, O (CH₂)₂), 3.12 – 3.00 (m, 4H, N(CH₂)₂), 2.40 (s, 3H); ¹³C NMR (126 MHz, DMSO- d_6) δ 166.99 (Thiazole-C2), 148.28 (Pyrazole-C5), 147.07 (Pyrazole-C3), 146.18 (Imine H), 138.75 (Ar-C), 132.39 (Ar-C), 129.54 (Ar-C), 128.79 (Ar-C), 128.52 (Ar-C), 128.09 (Ar-C), 127.34 (Ar-C), 126.38 (Ar-C), 125.41 (Ar-C), 125.06 (Ar-C), 124.48 (Ar-C), 124.39 (Ar-C), 124.24 (Ar-C), 119.81 (Ar-C), 114.96 (Ar-C), 110.83 (Thiazole-C5), 108.08 (Pyrazole-C4), 66.22 (O(CH₂)₂), 50.36 (N(CH₂)₂), 18.46 (CH₃); HRMS (M+H)⁺: 495.1967 (calculated) and 495.1967 (observed) for $C_{28}H_{26}N_6OS$

2.4.4. (E)-4-(3-methyl-1-phenyl-4-((2-(4-(p-tolyl)thiazol-2-yl) hydrazineylidene)methyl)-1H-pyrazol-5-yl)morpholine (6c)

FT-IR (cm⁻¹): 3323 (NH), 3046 (Ar-CH), 2967 (sp³-CH), 2850 (sp³-

Table 1
The physicochemical data of pyrazole and morpholine integrated thiazole hybrids (6a-6j).

| Entry | Ar (5a-5j) | Products (6a-6j) | Yield (%) | M.P. (°C) |
|-------|---------------------|----------------------|------------|---------------------|
| 6a | | H ₃ C N S | 82 | 208-210 |
| 6b | | H ₃ C N S | 80 | 215–217 |
| 6c | €—CH ₃ | H ₃ C N S | 78 | 240-242 |
| 6d | €——OCH ₃ | H ₃ C N S | 80 | 185–187 |
| 6e | ₹——F | H ₃ C N S | 78 | 192–194 |
| | | | Cont | inued on next nage) |

(continued on next page)

Table 1 (continued)

| Entry | Ar (5a-5j) | Products (6a-6j) | Yield (%) | M.P. (°C) |
|-------|--------------------------------------|-------------------------|------------|-----------|
| 6f | €—CI | HN S | 85 | 194–196 |
| 6 g | § — ⟨ _ > Br | H ₃ C N S Br | 87 | 188–190 |
| 6h | ₹ NO ₂ | H ₃ C N S | 90 | 210–212 |
| 6i | €—CF ₃ | H ₃ C N S | 84 | 190–193 |
| 6j | €——OCF3 | HN S OCF3 | 83 | 235–238 |

CH), 1623 (C=N), 1591 (C=C), 1539 (C=C), 1506 (C=C), 1477 (C=C), 1262 (C—O), 1171 (C—N), 1114 (C-C); 1H NMR (500 MHz, DMSO- d_6) δ 11.98 (s, 1H, NH), 8.35 (s, 1H, imine H), 7.73 (d, J=8.0 Hz, 2H, Ar-H), 7.62 (d, J=7.7 Hz, 2H, Ar-CH), 7.52 (t, J=7.8 Hz, 2H, Ar-CH), 7.40 (t, J=7.4 Hz, 1H, Ar-CH), 7.27-7.18 (m, 3H, Ar-CH and Thiazole H), 3.65-3.54 (m, 4H, O(CH₂)₂), 3.11-3.00 (m, 4H, N (CH₂)₂), 2.38 (s, 3H, CH₃), 2.33 (s, 3H); 13 C NMR (126 MHz, DMSO- d_6) δ 168.40 (Thiazole-C2), 147.08 (Pyrazole-C5), 138.74 (Pyrazole-C3), 129.27 (Imine C), 128.81 (Ar-C), 127.84 (Ar-C), 126.55 (Ar-C), 125.74 (Ar-C), 124.47 (Ar-C), 124.23 (Ar-C), 123.94 (Ar-C), 113.70 (Ar-C), 111.10 (Ar-C), 109.37 (Thiazole-C5), 107.33 (Pyrazole-C4), 66.19 (O (CH₂)₂), 50.38 (N(CH₂)₂), 20.76 (CH₃), 14.83 (CH₃); HRMS (M+H) $^+$:

459.1967 (calculated) and 459.1977 (observed) for $\mathrm{C}_{25}\mathrm{H}_{26}\mathrm{N}_{6}\mathrm{OS}$

2.4.5. (E)-4-(4-((2-(4-(4-methoxyphenyl)thiazol-2-yl)hydrazineylidene) methyl)-3-methyl-1-phenyl-1H-pyrazol-5-yl)morpholine (6d)

FT-IR (cm⁻¹): 3332 (NH), 3060 (Ar-CH), 2977 (\mathfrak{sp}^3 -CH), 2848 (\mathfrak{sp}^3 -CH), 1615 (C=N), 1588, 1538 (C=C), 1506 (C=C), 1253 (C—O), 1186 (C—N); ¹H NMR (500 MHz, DMSO- d_6) δ 11.95 (\mathfrak{s} , 1H, NH), 8.33 (\mathfrak{s} , 1H, Imine NH), 7.77 (\mathfrak{d} , J=8.7 Hz, 2H, Ar-CH), 7.62 (\mathfrak{d} , J=7.6 Hz, 2H, Ar-CH), 7.52 (\mathfrak{t} , J=7.8 Hz, 2H, Ar-CH), 7.40 (\mathfrak{t} , J=7.4 Hz, 1H, Ar-CH), 7.13 (\mathfrak{s} , 1H, Thiazole H), 6.99 (\mathfrak{d} , J=8.7 Hz, 2H, Ar-CH), 3.79 (\mathfrak{s} , 3H, OCH₃), 3.63 – 3.56 (\mathfrak{m} , 4H, O(CH₂)₂), 3.10 – 3.03 (\mathfrak{m} , 4H, N(CH₂)₂), 2.38 (\mathfrak{s} , 3H, CH₃); ¹³C NMR (126 MHz, DMSO- d_6) δ 168.31 (Thiazole-

C2), 159.18 (Ar-C-O), 148.41 (Pyrazole-C5), 147.19 (Pyrazole-C3), 138.75 (Imine C), 138.41 (Ar-C), 128.90 (Ar-C), 128.81 (Ar-C), 127.38 (Ar-C), 127.14 (Ar-C), 124.39 (Ar-C), 124.25 (Ar-C), 114.00 (Ar-C), 113.78 (Ar-C), 107.98 (Thiazole-C5), 101.49 (Pyrazole-C4), 66.20 (N (CH₂)₂), 55.13 (OCH₃), 50.29 (N(CH₂)₂), 14.83 (CH₃); HRMS (*M* + H)⁺: 475.1916 (calculated) and 475.1924 (observed) for C₂₅H₂₆N₆O₂S

2.4.6. (E)-4-(4-((2-(4-(4-fluorophenyl)thiazol-2-yl)hydrazineylidene) methyl)-3-methyl-1-phenyl-1H-pyrazol-5-yl)morpholine (6e)

FT-IR (cm⁻¹): 3389 (NH), 3142 (Ar-CH), 3053 (Ar-CH), 2839 (sp³-CH), 1628 (C=N), 1606 (C=C), 1510 (C=C), 1239 (C—O), 1167 (C—N), 1103 (C—C); ¹H NMR (500 MHz, DMSO- d_6) δ 11.96 (s, 1H, NH), 8.32 (s, 1H, Imine H), 7.89 (dd, J=8.6, 5.6 Hz, 2H, Ar-H), 7.65 – 7.60 (m, J=7.6 Hz, 2H, Ar-H), 7.52 (t, J=7.8 Hz, 2H, Ar-H), 7.40 (t, J=7.4 Hz, 1H, Ar-H), 7.28 – 7.22 (m, 3H, Ar-H and Thiazole H), 3.61 – 3.53 (m, 4H, O(CH₂)₂), 3.09 – 3.02 (m, 4H, N(CH₂)₂), 2.38 (s, 3H, CH₃); ¹³C NMR (126 MHz, DMSO- d_6) δ 168.35 (Thiazole-C2), 161.53 (d, J=244.5 Hz, Ar-C-F), 148.68 (Pyrazole-C5), 147.92 (Pyrazole-C3), 147.01 (Imine C), 138.80 (Ar-C), 136.13 (Ar-C), 130.90 (d, J=3.0 Hz, Ar-C(p to F), 128.76 (Ar-C), 127.47 (d, J=8.2 Hz, Ar-C(m to F),), 127.26 (Ar-C), 124.22 (Ar-C), 115.34 (d, J=21.5 Hz, Ar-C(m to F), 108.43 (Thiazole-C5), 102.86 (Pyrazole-C4), 66.22 (O(CH₂)₂), 50.24 (N(CH₂)₂), 14.71 (CH₃); HRMS (M+H)+: 463.17163 (calculated) and 463.172675.1924 (observed) for $C_{24}H_{23}FN_6OS$

2.4.7. (E)-4-(4-((2-(4-(4-chlorophenyl)thiazol-2-yl)hydrazineylidene) methyl)-3-methyl-1-phenyl-1H-pyrazol-5-yl)morpholine (6f)

FT-IR (cm⁻¹): 3350 (NH), 3047 (Ar-CH), 2860 (sp^3 -CH), 2835 (sp^3 -CH), 1635 (C=N), 1598 (C=C), 1267 (C—O), 1185 (C—N), 1110 (C—C); ¹H NMR (500 MHz, DMSO- d_6) δ 11.90 (s, 1H, NH), 8.29 (s, 1H, Imine H), 7.87 (d, J=8.5 Hz, 2H, Ar-H), 7.62 (d, J=7.6 Hz, 2H, Ar-H), 7.52 (t, J=7.8 Hz, 2H, Ar-H), 7.47 (d, J=8.5 Hz, 2H, Ar-H), 7.40 (t, J=7.4 Hz, 1H, Ar-H), 7.35 (s, 1H, Thiazole H), 3.63 – 3.56 (m, 4H, O (CH₂)₂), 3.11 – 3.02 (m, 4H, N(CH₂)₂), 2.38 (s, 3H, CH₃); ¹³C NMR (126 MHz, DMSO- d_6) δ 168.42 (Thiazole-C2), 148.07 (Pyrazole-C3), 147.07 (Imine C), 138.76 (Ar-C), 136.76 (Ar-C), 132.06 (Ar-C), 129.16 (Ar-C), 128.78 (Ar-C), 128.55 (Ar-C), 128.31 (Ar-C), 127.26 (Ar-C), 127.16 (Ar-C), 124.24 (Ar-C), 108.28 (Thiazole-C5), 104.07 (Pyrazole-C4), 66.22 (O(CH₂)₂), 50.25 (N(CH₂)₂), 14.75 (CH₃); HRMS (M+H)⁺: 479.1420 (calculated) and 479.1432 (observed), (M+H+2)⁺: 481.1577 (calculated) and 481.1407 (observed) for $C_{24}H_{23}$ ClN₆OS

2.4.8. (E)-4-(4-((2-(4-(4-bromophenyl)thiazol-2-yl)hydrazineylidene) methyl)-3-methyl-1-phenyl-1H-pyrazol-5-yl)morpholine (6g)

FT-IR (cm⁻¹): 3350 (NH), 3045 (Ar-CH), 2958 (sp³-CH), 1634 (C=N), 1598 (C=C), 1504 (C=C), 1267 (C—O), 1110 (C—C); ¹H NMR (500 MHz, DMSO- d_6) δ 11.86 (s, 1H, NH), 8.28 (s, 1H, Imine H), 7.80 (d, J=8.5 Hz, 2H, Ar-H), 7.63 – 7.59 (m, J=9.0 Hz, 4H, Ar-H), 7.52 (t, J=7.8 Hz, 2H, Ar-H), 7.40 (t, J=7.4 Hz, 1H, Ar-H), 7.37 (s, 1H, Thiazole H), 3.60 – 3.57 (m, 4H, O(CH₂)₂), 3.07 – 3.03 (m, 4H, N(CH₂)₂), 2.38 (s, 3H, CH₃); ¹³C NMR (126 MHz, DMSO- d_6) δ 168.41 (Thiazole-C2), 148.05 (Pyrazole-C5), 147.06 (Imine C), 138.76 (Ar-C), 136.67 (Ar-C), 133.15 (Ar-C), 131.45 (Ar-C), 129.44 (Ar-C), 128.78 (Ar-C), 127.55 (Ar-C), 127.30 (Ar-C), 124.23 (Ar-C), 120.64 (Ar-C), 108.29 (Thiazole-C5), 104.13 (Pyrazole-C4), 66.21 (O(CH₂)₂), 50.25 (N(CH₂)₂), 14.75 (CH₃); HRMS (M+H)+: 523.0915 (calculated) and 523.0921 (observed), (M+H+2)+: 525.1072 (calculated) and 525.0902 (observed) for $C_{24}H_{23}ClN_6OS$

2.4.9. (E)-4-(3-methyl-4-((2-(4-(4-nitrophenyl)thiazol-2-yl) hydrazineylidene)methyl)-1-phenyl-1H-pyrazol-5-yl)morpholine (6h)

FT-IR (cm⁻¹): 3323 (NH), 3082 (Ar-CH), 2957 (sp^3 -CH), 2895 (sp^3 -CH), 1594 (C = N), 1559 (C = C), 1496 (C = N), 1214 (C—O), 1107 (C—C); ¹H NMR (500 MHz, DMSO- d_6) δ 11.95 (s, 1H, NH), 8.31 – 8.26 (m, 3H, Imine H and Ar-H), 8.11 (d, J = 8.9 Hz, 2H, Ar-H), 7.68 (s, 1H, Thiazole H), 7.65 – 7.60 (m, 2H, Ar-H), 7.52 (t, J = 7.9 Hz, 2H, Ar-H),

7.40 (t, J=7.4 Hz, 1H, Ar-H), 3.63 – 3.56 (m, 4H, O(CH₂)₂), 3.10 – 3.02 (m, 4H, N(CH₂)₂), 2.38 (s, 3H, CH₃); ¹³C NMR (126 MHz, DMSO- d_6) δ 169.18 168.41 (Thiazole-C2), 148.86 (Pyrazole-C5), 148.48 (Imine C), 147.59 (Ar-C), 146.62 (Ar-C), 141.16 (Ar-C), 139.36 (Ar-C), 136.63 (Ar-C), 129.32 (Ar-C), 127.83 (Ar-C), 126.80 (Ar-C), 124.78 (Ar-C), 124.55 (Ar-C), 108.97 (Thiazole-C5), 108.54 (Pyrazole-C4), 66.80 (O(CH₂)₂), 50.81 (N(CH₂)₂), 15.29 (CH₃); HRMS (M+H)⁺: 490.1661 (calculated) and 490.1663 (observed) for C₂₄H₂₃N₇O₃S

2.4.10. (E)-4-(3-methyl-1-phenyl-4-((2-(4-(4-(trifluoromethyl)phenyl) thiazol-2-yl)hydrazineylidene)methyl)-1H-pyrazol-5-yl)morpholine (6i)

FT-IR (cm⁻¹): 3355 (NH), 3049 (Ar-CH), 2982 (sp³-CH), 2865 (sp³-CH), 1638 (C=N), 1597 (C=C), 1506 (C=C), 1173 (C—N), 1110 (C—C); ¹H NMR (500 MHz, DMSO- d_6) δ 11.92 (s, 1H, NH), 8.29 (s, 1H, Imine H), 8.07 (d, J=8.1 Hz, 2H, Ar-H), 7.77 (d, J=8.3 Hz, 2H, Ar-H), 7.62 (d, J=7.7 Hz, 2H, Ar-H), 7.53 (s, 1H, Thiazole H), 7.51 (d, J=8.0 Hz, 2H, Ar-H), 7.42 – 7.38 (m, 1H, Ar-H), 3.62 – 3.57 (m, 4H, O(CH₂)₂), 3.08 – 3.04 (m, 4H, N(CH₂)₂), 2.38 (s, 3H, CH₃); ¹³C NMR (126 MHz, DMSO- d_6) δ 169.08 (Thiazole-C2), 149.07 (Pyrazole-C5), 148.50 (Imine C), 147.59 (Ar-C), 139.36 (Ar-C), 138.70 (Ar-C), 136.68 (Ar-C), 130.52 (Ar-C), 128.14 (Ar-C), 125.91 (Ar-C), 123.75 (Ar-C), 108.97 (Thiazole-C5), 106.48 (Pyrazole-C4), 66.79 (O(CH₂)₂), 50.81 (N(CH₂)₂), 15.28 (CH₃); HRMS (M+H)+: 513.1684 (calculated) and 513.1695 (observed) for C₂₅H₂₃F₃N₆OS

2.4.11. (E)-4-(3-methyl-1-phenyl-4-((2-(4-(4-(trifluoromethoxy)phenyl) thiazol-2-yl)hydrazineylidene)methyl)-1H-pyrazol-5-yl)morpholine (6j)

FT-IR (cm⁻¹): 3356 (NH), 3067 (Ar-CH), 2955 (sp^3 -CH), 2863 (sp^3 -CH), 1637 (C=N), 1597 (C=C), 1505 (C=C), 1210 (C—O), 1167 (C—N), 1110 (C—C); ¹H NMR (500 MHz, DMSO- d_6) δ 11.90 (s, 1H, NH), 8.29 (s, 1H, Imine H), 7.97 (d, J=8.7 Hz, 2H, Ar-H), 7.64 – 7.61 (m, 2H, Ar-H), 7.54 – 7.50 (m, 2H, Ar-H), 7.42 – 7.36 (m, 4H, Ar-H and Thiazole H), 3.61 – 3.56 (m, 4H, O(CH₂)₂), 3.08 – 3.03 (m, 4H, N(CH₂)₂), 2.38 (s, 3H, CH₃); ¹³C NMR (126 MHz, DMSO- d_6) δ 169.02 (Thiazole-C2), 148.93 (Pyrazole-C5), 148.51 (Imine C), 148.05 (Ar-C), 148.04 (Ar-C), 147.59 (Ar-C), 139.36 (Ar-C), 136.75 (Ar-C), 134.17 (Ar-C), 129.33 (Ar-C), 127.83 (Ar-C), 124.80 (Ar-C), 121.68 (Ar-C), 119.56 (Ar-C), 108.97 (Thiazole-C5), 104.77 (Pyrazole-C4), 66.79 (O(CH₂)₂), 50.81 (N(CH₂)₂), 15.28 (CH₃); HRMS (M+H)⁺: 529.1633 (calculated) and 529.1644 (observed) for $C_{25}H_{23}F_{3}N_{6}O_{2}S$

2.5. DFT method

DFT method is widely used to analyze the electronic properties, stability, and reactivity of many small organic molecules offering insights for applications in chemistry and pharmacology [44–46]. All DFT computations for the synthesized compounds (**6a-6j**) were carried out in the gas phase using the Gaussian 03 software [47]. The calculations employed Becke's three-parameter hybrid exchange functional (B3LYP) [48,49] with the 6–31G(d,p) basis set. Molecular visualization was performed using the GaussView 4.1.2 program [50].

2.6. ADME study

The ADME study was conducted using online free software Swiss ADME [51].

2.7. Antitubercular study

The pyrazole and morpholine integrated thiazole hybrids (6a-6j) were screened for antitubercular activity against *Mycobacterium tuberculosis* H37Rv strain (ATCC 27,294) using the Microplate Alamar Blue Assay (MABA) [52]. This method is widely used due to its non-toxic nature, stability of the reagent, and strong correlation with proportional and BACTEC radiometric assays . The compounds were tested at concentrations ranging from 100 µg/mL to 0.2 µg/mL. A sterile 96-well

Scheme 2. Probable mechanism for the synthesis of pyrazole-thiazole hybrids (**6a-6j**) *via* thiosemicarbazone intermediate and cyclization with α-bromoacetophenone.

plate was prepared by adding 200 μL of sterile deionized water to the outer wells to reduce evaporation of the medium. Each test well was filled with 100 μL of Middlebrook 7H9 broth, and serial dilutions of the compounds were performed directly on the plate. The plates were covered, sealed with parafilm, and incubated at 37 °C for five days. After the incubation period, 25 μL of a freshly prepared 1:1 solution of Alamar Blue reagent and 10 % Tween 80 were added to each well and incubated for an additional 24 h. Wells that remained blue were interpreted as having no bacterial growth, while a pink color indicated growth. The minimum inhibitory concentration (MIC) was defined as the lowest concentration of the compound that inhibited bacterial growth, preventing the color change from blue to pink. Standard antitubercular drugs, including isoniazid (1.6 $\mu g/mL$), ethambutol (1.6 $\mu g/mL$), pyrazinamide (3.125 $\mu g/mL$), rifampicin (0.8 $\mu g/ml$), and streptomycin (0.8 $\mu g/mL$), were used as positive controls for reference.

2.8. Molecular docking studies

Molecular docking is an essential tool in contemporary drug discovery and development, offering valuable insights into the interactions between small molecules (ligands) and biological targets. For this study, docking simulations were performed using AutoDockTools 1.5.6 software [53], encompassing protein and ligand preparation, grid generation, and docking procedures. Ligand stability was achieved through energy minimization at the MM2 level using Chem3D Pro [54]. The three-dimensional crystal structures of proteins were sourced from the Protein Data Bank (https://www.rcsb.org/). To further explore binding dynamics, 2D and 3D ligand-receptor interactions were visualized and analyzed with Discovery Studio Visualizer (DSV) [55].

3. Results and discussion

3.1. Chemistry and spectral characterization

The synthesis of the target compounds (6a–6j) commenced with the preparation of compound 3. Compound 3 was synthesized by reacting compound 1 with morpholine (2) in the presence of potassium carbonate (K_2CO_3) as a base, using DMF as the solvent. The reaction proceeds via a nucleophilic substitution mechanism, wherein the chlorine atom in compound 1 is replaced by the morpholine. The target pyrazolethiazole derivatives (6a–6j) were synthesized through a two-step condensation reaction, as shown in Scheme 1. In the first step, compound 3 underwent condensation with thiosemicarbazide (4) in ethanol with catalytic acetic acid, resulting in the formation of a thiosemicarbazone intermediate. The reaction proceeded efficiently under reflux conditions for 1 h, leading to imine (-C = N) formation. Acetic acid promoted protonation, enhancing the electrophilicity of the

carbonyl carbon of compound 3 and facilitating the condensation. In the second step, the thiosemicarbazone intermediate was reacted with aryl bromoketones ($\bf 5a-5j$), facilitating cyclization to form the thiazole ring and yielding the final pyrazole-thiazole hybrids ($\bf 6a-6j$). The reaction followed the typical Hantzsch thiazole synthesis mechanism [$\bf 56,57$], in which the nucleophilic sulfur of the thiosemicarbazone intermediate attacked the electrophilic α -carbon of the aryl bromoketones, resulting in cyclization and HBr elimination. The reaction progress was monitored by TLC until complete conversion. The final products precipitated as solids, which were filtered, washed with cold ethanol to remove impurities, and dried to obtain pure $\bf 6a-6j$ in good yields. The probable mechanism based on previous study [$\bf 57,58$], is depicted in Scheme 2.

The spectral analysis confirms the structural units in the synthesized compounds [59,60]. The spectral data of 3-methyl-5-morpholino-1-phenyl-1H-pyrazole-4-carbaldehyde confirms its structure. In the ^{1}H NMR spectrum, a singlet at δ 9.95 ppm indicates the aldehyde proton, while aromatic protons appear as multiplets at 7.61–7.42 ppm (5H). The morpholine ring protons resonate at 3.58–3.54 ppm (4H) and 3.11-3.07 ppm (4H), and a singlet at 2.36 ppm corresponds to the pyrazole methyl group. The ¹³C NMR spectrum shows the carbonyl carbon at δ 183.80 ppm, with pyrazole and phenyl carbons between 152.03-111.94 ppm, morpholine carbons at 65.87 and 50.37 ppm, and the methyl carbon at 13.65 ppm, confirming the synthesized structure. The structural confirmation of the synthesized (E)-4-(3-methyl-1-phenyl-4-((2-(arylthiazol-2-yl)hydrazineylidene) methyl)-1H-pyrazol-5-yl)morpholine derivatives (6a-6j) was achieved through FT-IR, ¹H NMR, ¹³C NMR and HRMS spectral methods. The FT-IR spectrum displays characteristic absorption bands corresponding to key functional groups. A strong band in the range of 1590–1625 cm is assigned to C = N stretching vibration of the azomethine moiety, confirming the formation of the Schiff base. The presence of the thiazole ring is further supported by bands observed in the range of 1350-1450 ${\rm cm}^{-1}$, attributed to the C–N and C–S stretching vibrations. Aromatic C=C stretching vibrations appear in the region of $1450-1600 \text{ cm}^{-1}$. The morpholine ring is confirmed by the presence of aliphatic C-N stretching bands around 1100 cm⁻¹ and C-O-C stretching in the range of 1200 cm⁻¹. The presence of a broad N-H stretching band indicates successful formation of NH—C = N. The ¹H NMR spectral analysis further supports the structure, showing a characteristic singlet in the 8.5–9.2 ppm range for the azomethine (-CH \equiv N-) proton, confirming the presence of the imine linkage. The singlet peak observed around $\delta\ 11.86\text{--}11.98\ ppm$ corresponds to the NH proton, confirming the presence of the thiosemicarbazone (-NH) moiety. The aromatic protons of the phenyl and thiazole rings resonate as multiple signals between 6.8-8.2 ppm. The pyrazole C5–H proton appears as a sharp singlet in the range of 7.5–8.0 ppm, supporting the substituted pyrazole framework. The morpholine protons appear as broad signals in the 3.2-3.8 ppm range, while the

Table 2 Antitubercular activity of pyrazole and morpholine integrated thiazole hybrids (6a-6j).

| | • |
|------------|-------------|
| Entry | MIC (μg/mL) |
| 6a | 100 |
| 6b | 100 |
| 6c | 50 |
| 6d | 25 |
| 6e | 50 |
| 6f | 50 |
| 6g | 50 |
| 6h | 100 |
| 6i | 12.5 |
| 6 j | 50 |

methyl group attached to the pyrazole ring resonates as a singlet at 2.3–2.5 ppm.

The ¹³C NMR spectra of compounds **6a–6j** exhibit characteristic chemical shifts corresponding to their structural features, confirming

their successful synthesis. Across all compounds, signals around δ 168–169 are consistently assigned to the C2 carbon of the thiazole ring, indicative of the electron-deficient nature of this position. The pyrazole ring carbons—C5 and C3—typically resonate between δ 147–149, while the C4 pyrazole carbon appears further upfield between δ 101–108. The imine carbon (C = N) shows deshielded signals around δ 138–146, supporting the formation of the hydrazone linkage. Substituted aryl groups contribute multiple signals in the aromatic region, varying with electron-withdrawing or electron-donating substituents. For instance, in compound 6e, the fluorinated phenyl ring shows characteristic coupling in the 13 C NMR with peaks like δ 161.53 (d, J=244.5 Hz) for the C-F carbon and δ 115.34 (d, J=21.5 Hz) for the ortho carbon, confirming fluorine substitution. Similarly, methoxy-substitution in 6d results in a distinct peak at δ 159.18 (Ar–C–O) and δ 55.13 for the OCH3 group. The morpholine ring methylene carbons consistently appear at δ 66–67 (O-CH₂) and δ 50–51 (N-CH₂). Methyl groups, either on the pyrazole or the aromatic ring, appear in the δ 14–21 range, with higher values ($\sim\!20$ δ) typically for *p*-tolyl or electron-donating substitutions. The 13 C NMR

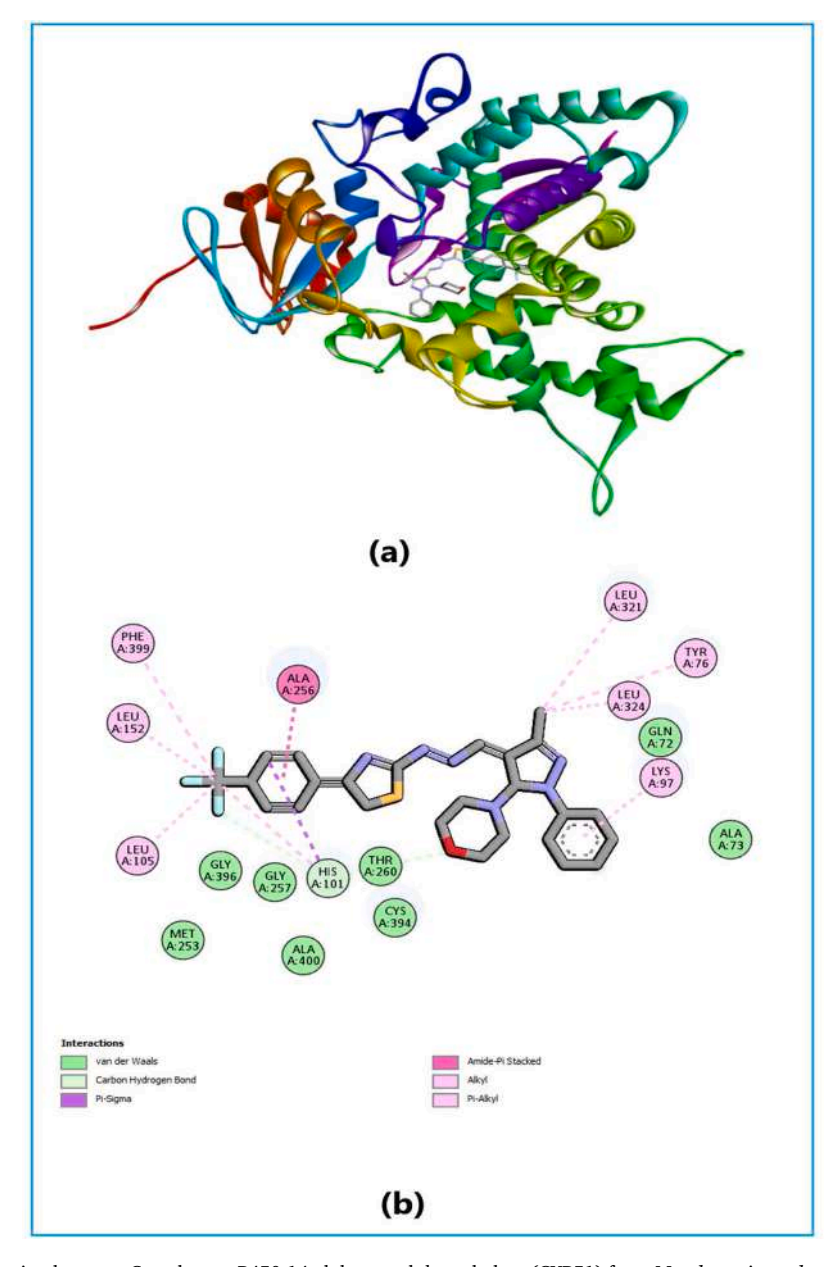


Fig. 2. (a and b) Binding interaction between Cytochrome P450 14 alpha-sterol demethylase (CYP51) from Mycobacterium tuberculosis (PDB ID: 1E9X) protein and compound 6i.

data across compounds **6a–6j** not only corroborate the expected chemical structures but also demonstrate the electronic influences of the aryl substituents on the chemical shifts, particularly in the aromatic and heteroaromatic regions. These spectral patterns validate the substitution effects and the integrity of the synthesized conjugated heterocyclic frameworks.

The HRMS data of compounds **6a–6j** confirm their molecular integrity and successful synthesis, as evidenced by the excellent agreement between the calculated and observed $[M+H]^+$ values. The compound **6a** exhibited a calculated m/z of 445.1810 and was observed at 445.1818, while compound **6b** matched exactly at 495.1967. Similar high accuracy was observed across the series, including **6c** (459.1977), **6d** (475.1924), **6e** (463.1726), **6h** (490.1663), **6i** (513.1695), and **6j** (529.1644). The compounds containing halogens displayed characteristic isotopic patterns: **6f** showed peaks at m/z 479.1432 and 481.1407 (M+2), confirming the presence of chlorine due to its natural isotopic abundance (35 Cl and 37 Cl in \sim 3:1 ratio), while **6g** exhibited peaks at m/z 523.0921 and 525.0902 (M+2), indicative of bromine (79 Br and 81 Br in \sim 1:1 ratio). These observations collectively validate the proposed molecular formulae and the structural integrity of the synthesized compounds.

3.2. Antitubercular activity

The antitubercular activity of the synthesized pyrazole and morpholine-integrated thiazole hybrids (6a-6j) was assessed against Mycobacterium tuberculosis H37Rv strain, and their minimum inhibitory concentration (MIC) values are provided in Table 2. The results reveal significant variation in antitubercular activity depending on the nature and position of substituents on the phenyl ring attached to the thiazole core. Among the tested compounds, 6i displayed the most potent activity with an MIC value of 12.5 $\mu g/mL$, highlighting the critical role of the trifluoromethyl group at the para position of the phenyl ring in enhancing the antitubercular efficacy. The strong electron-withdrawing nature of the trifluoromethyl group is known to improve lipophilicity and facilitate better interaction with the target site, thereby boosting activity. Compound 6d also demonstrated notable antitubercular activity with an MIC of 25 µg/mL, which can be attributed to the presence of a methoxy group at the para position of the phenyl ring. The electrondonating effect of the methoxy group may favorably influence the binding affinity to the bacterial target. In contrast, compounds 6c, 6e, 6f, 6 g, and 6j exhibited moderate activity with an MIC of 50 µg/mL,

 $\begin{array}{ll} \textbf{Table 3} \\ \textbf{Physicochemical properties, pharmacokinetics, and drug-likeness} \\ \textbf{evaluation of the compound 6i.} \end{array}$

| Property | Value |
|---------------------------|--------------|
| Molecular Weight | 512.55 g/mol |
| Num. Heavy Atoms | 36 |
| Num. Aromatic Heavy Atoms | 22 |
| Num. H-bond Acceptors | 7 |
| Num. H-bond Donors | 1 |
| Molar Refractivity | 137.84 |
| TPSA | 95.81 Ų |
| Log Po/w (SILICOS-IT) | 5.64 |
| Consensus Log Po/w | 5.05 |
| Log S (ESOL) | -6.73 |
| GI absorption | Low |
| BBB permeant | No |
| P-gp substrate | Yes |
| CYP1A2 inhibitor | No |
| CYP2C19 inhibitor | Yes |
| CYP2C9 inhibitor | Yes |
| CYP2D6 inhibitor | Yes |
| CYP3A4 inhibitor | Yes |
| Lipinski | Yes |
| Ghose | No |
| Veber | Yes |

indicating that halogen substitutions such as fluoro, chloro, bromo, and trifluoromethoxy groups provide moderate improvements in antitubercular potency. These halogen atoms, being moderately electronwithdrawing, are known to enhance the pharmacokinetic properties and improve molecular stability, contributing to moderate efficacy. On the other hand, compounds 6a, 6b, and 6h, featuring phenyl, naphthyl, and nitrophenyl substitutions, showed relatively low activity with an MIC of 100 µg/mL. The simple phenyl ring in 6a lacks any electronwithdrawing or donating substituent, which may explain its reduced activity. Similarly, the naphthyl group in 6b likely introduces steric hindrance, impairing effective binding to the bacterial enzyme or target site. Compound 6h, containing a nitrophenyl group, also exhibited weak activity, possibly due to decreased bioavailability or unfavorable electronic interactions. These findings suggest that the presence of electronwithdrawing substituents like trifluoromethyl and halogens at the para position of the phenyl ring plays a crucial role in improving antitubercular activity, likely by enhancing lipophilicity and binding affinity. In contrast, simple phenyl groups or bulky naphthyl moieties reduce the efficacy due to steric or electronic factors. The compound 6i stands out as the most promising molecule in this series, warranting further structural modifications and detailed mechanistic studies to optimize its antitubercular activity and pharmacological profile.

3.3. Molecular docking investigation

A key player in sterol biosynthesis, cytochrome P450 14α-sterol demethylase (CYP51) is a desirable therapeutic target for antitubercular drug discovery. This enzyme is necessary for preserving membrane stability and functionality; its inhibition compromises the sterol biosynthesis pathway, which in turn impairs membrane integrity and ultimately results in cell death [61-63]. Consequently, CYP51 inhibition in Mycobacterium tuberculosis is a promising approach for developing new antitubercular agents. Compound 6i shows notable binding affinity with CYP51 due to its unique structural features, including a pyrazole-thiazole core, a trifluoromethyl-substituted phenyl ring, and a morpholine moiety (Figs. 2a and 2b). These functional groups facilitate various interactions, such as hydrogen bonding, hydrophobic interactions, and π -stacking, which contribute to its strong binding affinity (-8.9 kcal/mol) and selectivity for CYP51. Hydrogen bonding plays a significant role in stabilizing compound 6i within the active site of CYP51. Specifically, two hydrogen bonds involving His101 were observed. The first interaction with His101:CD2 at a distance of 2.93 Å forms a carbon-hydrogen bond, which helps orient the ligand within the binding site. The second hydrogen bond occurs at His101:CE1, with a bond length of 3.12 Å, further stabilizing the ligand's position. These interactions highlight His101 as a key residue in maintaining the ligand's proper orientation and stability within the binding pocket. Beyond hydrogen bonding, hydrophobic contacts also significantly enhance the binding strength of compound 6i. A notable π -sigma interaction with His101 (3.92 Å) provides additional stabilization through π -stacking. Furthermore, an amide- π stacking interaction with Ala256 and Gly257 (4.14 Å) indicates that the ligand's aromatic system interacts favorably with the amide groups of these residues, contributing to its overall stability. The examination reveals multiple alkyl and π -alkyl interactions with hydrophobic residues, including Leu105, Leu152, Leu321, and Leu324, with interaction distances ranging from 4.49 to 5.20 Å. These hydrophobic contacts help anchor the ligand within the pocket and enhance its binding affinity. Additionally, Phe399 engages in a π -alkyl interaction (4.95 Å) with the aromatic portion of compound 6i, while Tyr76 and Lys97 further stabilize the complex through similar interactions. The trifluoromethyl group on the phenyl ring boosts the lipophilicity of compound 6i, reinforcing its hydrophobic interactions. Geometric parameters such as Theta, Theta 2, Gamma, and the closest atom distance support the favorable binding conformation of compound 6i within the CYP51 active site. The observed Theta and Theta 2 values of 31.6° and 29.2°, respectively, suggest optimal angular

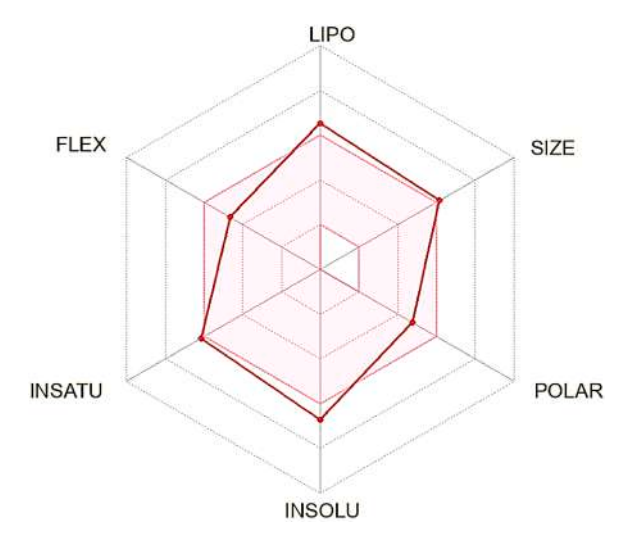


Fig. 3. Radar plot of compound **6i** representing molecular descriptors: lip-ophilicity (LIPO), size, polarity (POLAR), insolubility (INSOLU), saturation (INSATU), and flexibility (FLEX).

positioning for forming robust hydrogen bonds and hydrophobic contacts, thereby avoiding steric clashes and ensuring proper ligand orientation. The closest atom distance of 3.62 Å indicates a close interaction between the ligand and key amino acid residues, further confirming strong binding. The electron-rich pyrazole-thiazole core facilitates π -stacking interactions with aromatic residues such as His101 and Phe399, adding to the overall stability of the ligand-receptor complex. This extensive interaction profile suggests that compound 6i may function as a CYP51 inhibitor, disrupting sterol biosynthesis and exhibiting potential antitubercular activity. Molecular docking studies highlight the promising binding interactions of compound 6i, making it a potential lead for further drug development.

3.4. Physicochemical properties, pharmacokinetics, and drug-likeness evaluation

The physicochemical properties and pharmacokinetics of the compound 6i were evaluated for its drug-likeness and therapeutic potential (Table 3). The compound's 36 heavy atoms and 22 aromatic heavy atoms contribute to its rigidity and lipophilic nature. The molar refractivity (137.84) and TPSA (95.81 Å²) suggest moderate polarity and possible biological target interactions. The Log Po/w (SILICOS-IT) of 5.64 and consensus Log Po/w of 5.05 indicate high lipophilicity, enhancing membrane permeability but reducing water solubility (Log S= -6.73). Poor aqueous solubility may limit bioavailability, requiring formulation strategies for improvement. Pharmacokinetics revealed low GI absorption and non-permeability across the BBB, suggesting limited CNS penetration. As a P-gp substrate, the compound may have restricted intracellular accumulation. It inhibits CYP2C19, CYP2C9, CYP2D6, and CYP3A4, implying potential drug-drug interactions. Drug-likeness analysis shows it meets Lipinski's rule (with one violation for molecular weight) and Veber's criteria, but fails Ghose's filter due to high molecular weight and lipophilicity. These findings suggest further optimization is needed to improve solubility and bioavailability while retaining activity. The radar plot (Fig. 3) highlights the molecule's high lipophilicity and low solubility, which may improve membrane permeability but reduce aqueous solubility. The bioavailability plot (Fig. 4) indicates low gastrointestinal absorption and non-permeability across the blood-brain barrier (BBB). The ADME data of other compounds is given in supporting information. The series of compounds 6a-6j generally exhibit favorable ADME profiles characterized by high gastrointestinal absorption and moderate bioavailability scores around 0.55. Most compounds comply with Lipinski and Veber rules, indicating good druglikeness, although some show violations related to molecular weight, lipophilicity, or polar surface area, particularly compounds 6g, 6h, and 6j. All compounds are poorly soluble or moderately soluble, show limited or no blood-brain barrier permeability, and are substrates for P-glycoprotein (except 6h). They consistently inhibit multiple CYP450 enzymes such as CYP2C19, CYP2C9, CYP2D6, and CYP3A4, which may affect metabolism and drug interactions. Medicinal chemistry alerts are minimal, with none showing PAINS alerts, but all compounds have at least one Brenk alert mostly related to the presence of an

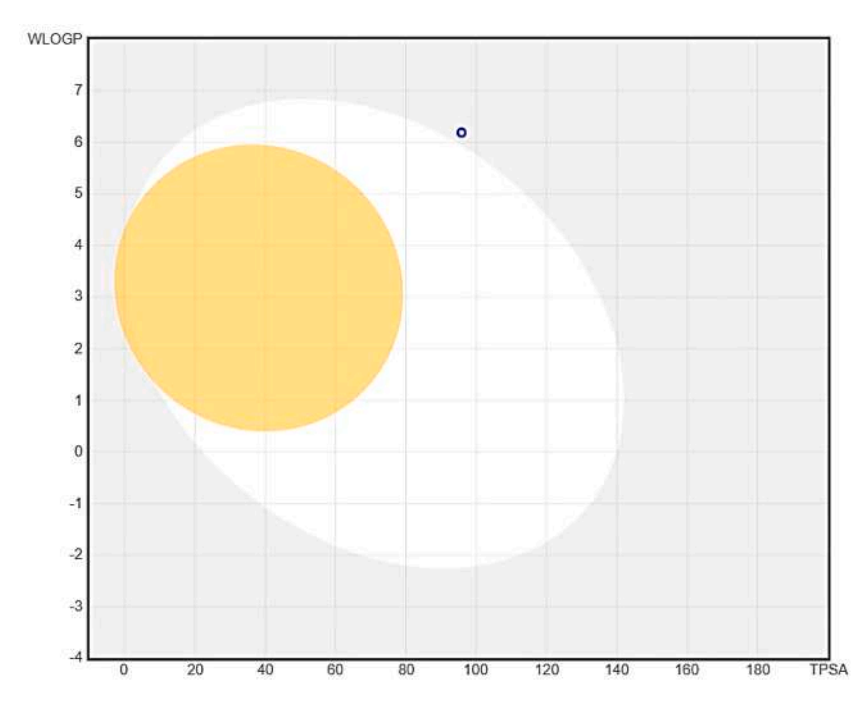


Fig. 4. BOILED-egg model of compound 6i for predicting gastrointestinal absorption and blood-brain barrier permeation based on WLOGP and TPSA Values.

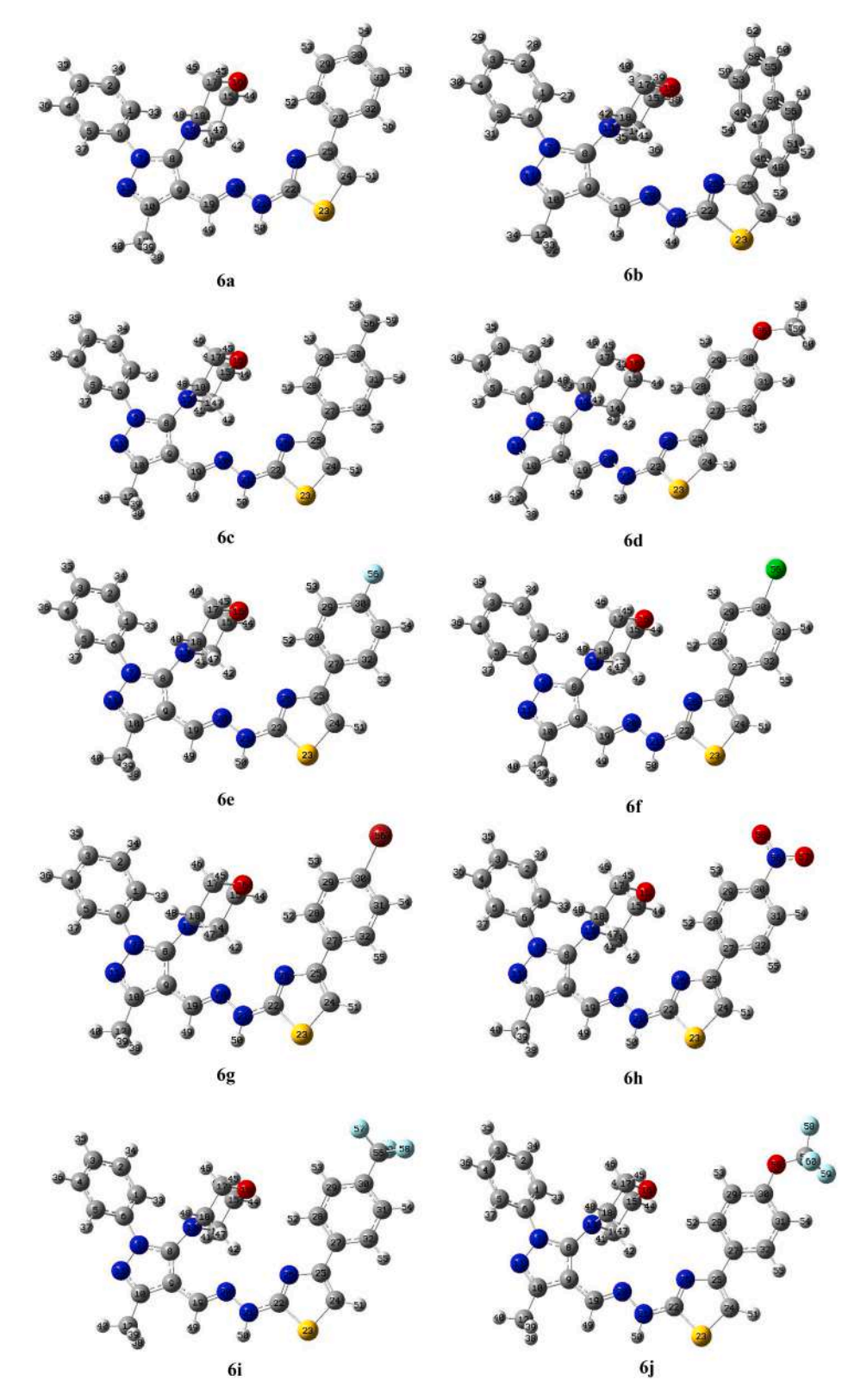


Fig. 5. Optimized structures of synthesized derivatives (6a-6j).

imine group; compound $\bf 6h$ additionally carries alerts for nitro and oxygen-nitrogen bonds.

3.5. DFT study

3.5.1. Optimized molecular structures, bond length analysis and structural insights

The DFT predicted geometries provide stable molecular structure for various small organic molecules [64,65]. The synthesized derivatives

Table 4
Bond length analysis of compound 6i.

| Bond | Bond length (Å) | Bond | Bond length (Å) | Bond | Bond length (Å) |
|---------|--------------------|---------|--------------------|---------|--------------------|
| C1-C2 | 1.3944 | C12-H39 | 1.096 | C22-S23 | 1.7753 |
| C1-C6 | 1.3983 | C12-H40 | 1.0919 | C22-N26 | 1.2956 |
| C1-H33 | 1.0813 | N13-C14 | 1.4754 | S23-C24 | 1.7455 |
| C2-C3 | 1.3955 | N13-C18 | 1.4762 | C24-C25 | 1.3691 |
| C2-H34 | 1.0859 | C14-C15 | 1.5272 | C24-H51 | 1.0791 |
| C3-C4 | 1.3959 | C14-H41 | 1.0956 | C25-C26 | 1.3877 |
| C3-H35 | 1.0857 | C14-H42 | 1.0975 | C25-C27 | 1.4758 |
| C4-C5 | 1.3932 | C15-O16 | 1.4243 | C27-C28 | 1.4045 |
| C4-H36 | 1.0859 | C15-H43 | 1.1023 | C27-C32 | 1.4056 |
| C5-C6 | 1.3989 | C15-H44 | 1.0935 | C28-C29 | 1.3914 |
| C5-H37 | 1.0833 | O16-C17 | 1.425 | C28-H52 | 1.0832 |
| C6-N7 | 1.4267 | C17-C18 | 1.5265 | C29-C30 | 1.3963 |
| N7-C8 | 1.3758 | C17-H45 | 1.0935 | C29-H53 | 1.0845 |
| N7-N11 | 1.3625 | C17-H46 | 1.1015 | C30-C31 | 1.399 |
| C8-C9 | 1.4043 | C18-H47 | 1.0991 | C30-C56 | 1.502 |
| C8-N13 | 1.4019 | C18-H48 | 1.0947 | C31-C32 | 1.3896 |
| C9-C10 | 1.4259 | C19-N20 | 1.2884 | C31-H54 | 1.0847 |
| C9-C19 | 1.4461 | C19-H49 | 1.0988 | C32-H55 | 1.0854 |
| C10-N11 | 1.3261 | N20-N21 | 1.3581 | C56-F57 | 1.352 |
| C10-C12 | 1.4983 | N21-C22 | 1.3723 | C56-F58 | 1.3537 |
| C12-H38 | 1.096 | N21-H50 | 1.016 | C56-F59 | 1.356 |

Table 5Mulliken atomic charges of compound 6i.

| Atom | Charge | Atom | Charge | Atom | Charge |
|------|----------|------|----------|------|----------|
| 1 C | -0.06336 | 21 N | -0.41081 | 41 H | 0.096621 |
| 2 C | -0.10792 | 22 C | 0.345266 | 42 H | 0.147373 |
| 3 C | -0.07614 | 23 S | 0.201788 | 43 H | 0.086589 |
| 4 C | -0.10086 | 24 C | -0.35309 | 44 H | 0.109704 |
| 5 C | -0.07525 | 25 C | 0.29606 | 45 H | 0.107854 |
| 6 C | 0.271997 | 26 N | -0.49393 | 46 H | 0.093733 |
| 7 N | -0.41433 | 27 C | 0.085544 | 47 H | 0.133939 |
| 8 C | 0.483072 | 28 C | -0.1306 | 48 H | 0.104543 |
| 9 C | -0.02596 | 29 C | -0.11947 | 49 H | 0.070537 |
| 10 C | 0.281607 | 30 C | -0.03359 | 50 H | 0.260489 |
| 11 N | -0.36054 | 31 C | -0.11351 | 51 H | 0.131216 |
| 12 C | -0.38007 | 32 C | -0.12609 | 52 H | 0.144394 |
| 13 N | -0.5575 | 33 H | 0.098141 | 53 H | 0.114497 |
| 14 C | -0.0542 | 34 H | 0.090922 | 54 H | 0.103749 |
| 15 C | 0.051002 | 35 H | 0.088778 | 55 H | 0.081169 |
| 16 O | -0.48113 | 36 H | 0.091891 | 56 C | 0.78219 |
| 17 C | 0.050993 | 37 H | 0.113034 | 57 F | -0.27166 |
| 18 C | -0.04876 | 38 H | 0.121247 | 58 F | -0.27415 |
| 19 C | 0.090954 | 39 H | 0.119418 | 59 F | -0.26464 |
| 20 N | -0.25102 | 40 H | 0.138262 | - | - |

(6a-6j) were theoretically studied to determine various structural and chemical parameters using DFT with the B4LYP functional and the 6-31G(d,p) basis set. The optimized geometries of all ten derivatives are depicted in Fig. 5. The bond length analysis of compound 6i depicted in Table 4 provides essential information about its molecular geometry and structural stability. The carbon-carbon bond lengths in the aromatic ring (C1-C2: 1.3944 Å, C2-C3: 1.3955 Å, C3-C4: 1.3959 Å) are typical for conjugated systems, indicating delocalization of π -electrons, which contributes to the ring's stability. Notably, the bond length between C22–S23 (1.7753 Å) and S23–C24 (1.7455 Å) reflects the presence of a thioether group, with slightly elongated bonds due to the sulfur atom's larger atomic radius. The C15-O16 bond (1.4243 Å) and O16-C17 (1.425 Å) suggest partial double-bond character, indicating conjugation with the adjacent system, which enhances the molecule's electron delocalization. The N7-C8 (1.3758 Å) and N7-N11 (1.3625 Å) bonds demonstrate the characteristic bond lengths of a pyrazole ring, confirming the heteroaromatic framework. C56-F57, C56-F58, and C56–F59 bonds range from 1.352 to 1.356 Å, indicating the presence of trifluoromethyl substitution, which significantly changes the compound's electronic properties by enhancing its electron-withdrawing

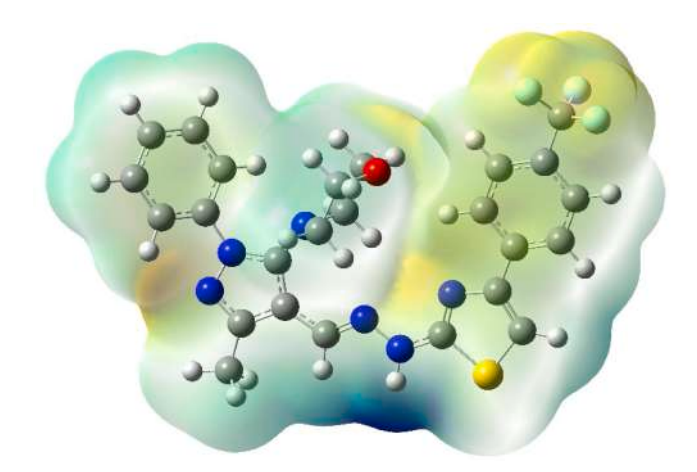


Fig. 6. Molecular electrostatic potential (MESP) map of compound 6i highlighting electron density distribution and reactive sites.

capacity. This substitution plays a critical role in the overall lipophilicity and biological activity of the molecule. Additionally, the presence of relatively long bonds such as C27–C32 (1.4056 Å) and C30–C56 (1.502 Å) indicates possible flexibility in these regions of the molecule, which may influence its binding conformation in biological environments. These bond lengths, combined with the Mulliken charge analysis, offer valuable insights into the compound's chemical reactivity and potential interaction sites, which are crucial for its antitubercular activity.

3.5.2. Mulliken charge distribution analysis

The molecule's reactive centres by Mulliken charge distribution analysis offer vital information on the molecule's chemical reactivity [66,67]. Using the DFT approach at the B3LYP/6-31G(d,p) level, the Mulliken charge analysis of compound 6i reveals insight into the distribution of electron densities throughout the molecule (Table 5). Significant negative charges render nitrogen atoms like N13 (-0.5575) and N26 (-0.4939) particularly electron-rich as well as prospective locations for electrophilic interactions. The oxygen atom O16 (-0.4811) is likewise quite electron-dense, which indicates that it has a significant ability to receive hydrogen bonds. Several carbon atoms, on the other hand, such as C6 (0.2719), C10 (0.2816), and especially C56 (0.7822), exhibit positive charges, which suggests an electron scarcity and a propensity for nucleophilic attack. The high positive charge on C56 is due to its connection with electronegative fluorine atoms (F57, F58, F59), which exhibit negative charges ranging from -0.2646 to -0.2741, further enhancing the electron-withdrawing effect. While the hydrogen atoms display varied degrees of positive charge, with H50 (0.2605) being the most positively charged and hence a favourable site for hydrogen bonding, the sulphur atom S23 (0.2018) has a moderate positive charge, showing partial electron donation to neighbouring carbons.

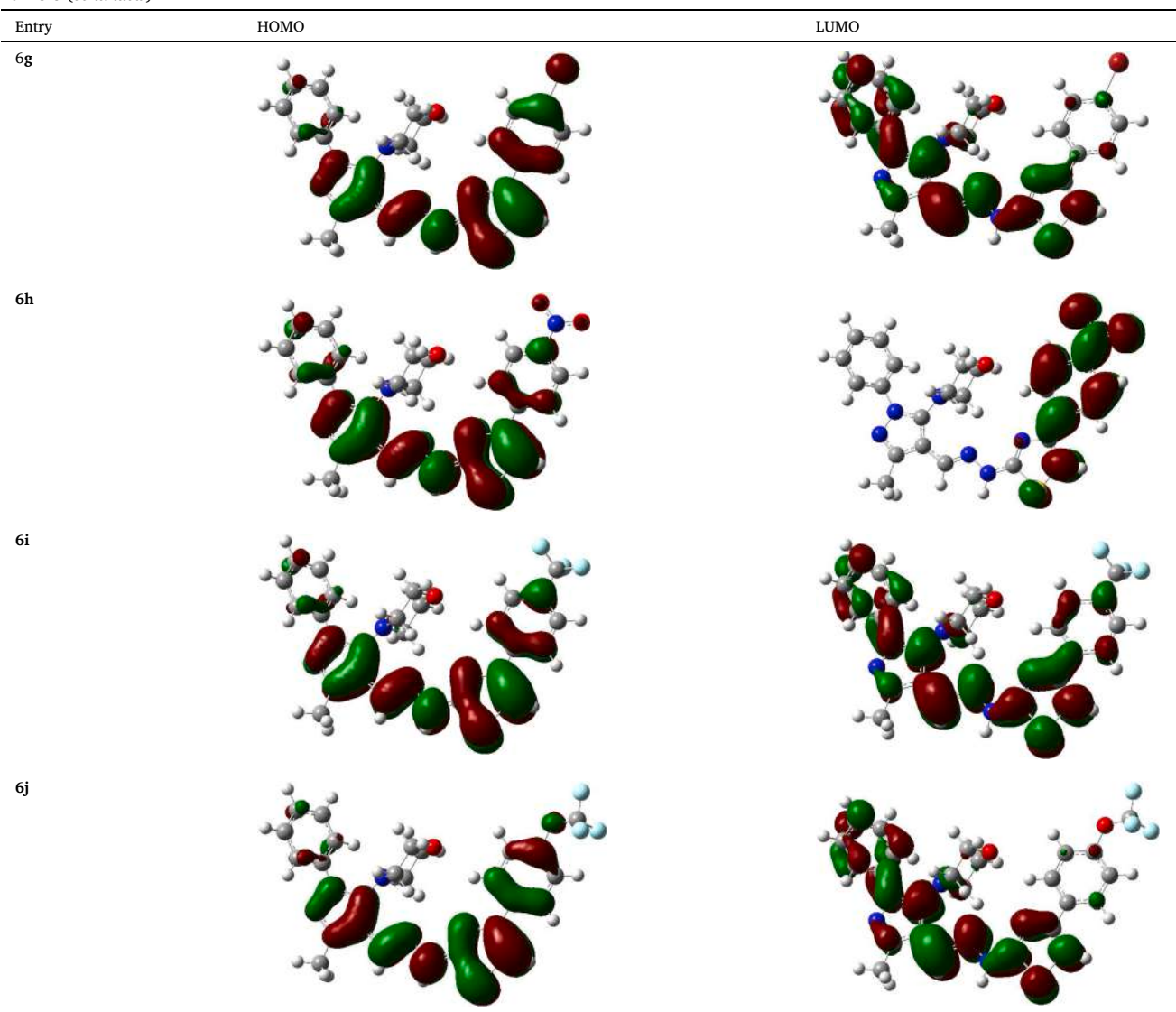
3.5.3. Molecular electrostatic potential (MESP) analysis

The electron density distribution and electrostatic potential throughout the molecule are shown in detail by the molecular electrostatic potential (MESP) map of compound **6i** (Fig. 6). This information is essential for locating reactive sites, electrophilic and nucleophilic areas, and the general molecular polarity [68,69]. Nucleophilic sites that are more likely to draw electrophiles are indicated by the red zones on the MESP map, which represent areas of high electron density [70]. Typically, electronegative elements like nitrogen and oxygen are linked to these red areas. The faint red or yellow region in compound **6i** that surrounds the nitrogen atoms in the pyrazole and thiazole rings and the oxygen atom in the morpholine ring draws attention to these putative nucleophilic sites. In contrast, low electron density regions are

Table 6
Frontier molecular orbitals of the synthesized compounds (6a-6j).

| Entry | НОМО | LUMO |
|-------|------|--------------------------|
| ба | | |
| 6b | | |
| 6c | | |
| 6d | | |
| бе | | |
| 6f | | |
| | | (continued on next page) |

Table 6 (continued)



represented by the blue areas, which indicate electrophilic sites. On the other hand, low electron density regions, which are shown by the blue regions, indicate electrophilic locations that are more prone to draw nucleophiles. The majority of these blue areas are found around hydrogen atoms that are joined to carbon and nitrogen atoms, indicating potential nucleophilic attack contact sites. Areas of intermediate electrostatic potential, which are comparatively neutral or less reactive regions in the molecule, are shown by the green and yellow sections. These areas are primarily located along the molecular backbone and on aromatic rings, such as the phenyl and trifluorophenyl groups. The MESP map identifies the functional groups in charge of molecular interactions and validates the distribution of electron densities throughout the heterocyclic scaffold.

3.5.4. Frontier molecular orbital analysis

Frontier Molecular Orbitals (FMOs) play a crucial role in understanding the chemical behavior and reactivity of molecules [71]. The two primary FMOs are the Highest Occupied Molecular Orbital (HOMO) and the Lowest Unoccupied Molecular Orbital (LUMO). The HOMO represents the molecular orbital with the highest energy that contains electrons, making it vital for assessing a molecule's ability to donate electrons. A higher (more negative) E_{HOMO} value indicates greater electron-donating potential and increased reactivity toward

Table 7Electronic parameters of the synthesized compounds (**6a-6j**).

| Entry | E (a.u.) | E _{HOMO} (eV) | E _{LUMO} (eV) | I (eV) | A (eV) | E _g (eV) | Dipole moment (Debye) |
|------------|----------|---------------------------|---------------------------|-----------|-----------|------------------------|-----------------------------|
| 6a | -1730.89 | -5.13 | -1.20 | 5.13 | 1.2 | 3.93 | 2.0281 |
| 6b | -1884.53 | -5.19 | -1.21 | 5.19 | 1.21 | 3.98 | 2.0718 |
| 6c | -1720.21 | -5.08 | -1.18 | 5.08 | 1.18 | 3.9 | 1.5445 |
| 6d | -1845.42 | -4.96 | -1.14 | 4.96 | 1.14 | 3.82 | 1.3451 |
| 6e | -1830.12 | -5.18 | -1.25 | 5.18 | 1.25 | 3.93 | 3.4159 |
| 6f | -2190.49 | -5.26 | -1.29 | 5.26 | 1.29 | 3.97 | 4.2579 |
| 6 g | -4302.00 | -5.25 | -1.29 | 5.25 | 1.29 | 3.96 | 4.2035 |
| 6h | -1935.40 | -5.50 | -2.22 | 5.5 | 2.22 | 3.28 | 7.8696 |
| 6i | -2067.93 | -5.35 | -1.34 | 5.35 | 1.34 | 4.01 | 5.2394 |
| 6j | -2143.15 | -5.25 | -1.29 | 5.25 | 1.29 | 3.96 | 4.4382 |

electrophiles, while a lower E_{HOMO} suggests reduced electron density and lower reactivity. Conversely, the LUMO, which is the lowest energy orbital available to accept electrons, is critical for evaluating a molecule's electron-accepting capability. A lower E_{LUMO} (less negative) corresponds to a higher likelihood of electron acceptance and increased reactivity toward nucleophiles. Table 6 displays the frontier molecular orbitals (FMOs) of the synthesized compounds (6a-6j).

 Table 8

 Global reactivity parameters of synthesized compounds.

| Entry | X (eV) | η (eV) | σ (eV ⁻¹) | ω (eV) | μ (eV) | ΔNmax (eV) |
|------------|--------|--------|-----------------------|--------|--------|------------|
| 6a | 3.16 | 1.96 | 0.51 | -3.16 | 2.55 | 1.61 |
| 6b | 3.2 | 1.99 | 0.5 | -3.2 | 2.57 | 1.61 |
| 6c | 3.13 | 1.95 | 0.51 | -3.13 | 2.51 | 1.61 |
| 6d | 3.05 | 1.91 | 0.52 | -3.05 | 2.44 | 1.60 |
| 6e | 3.22 | 1.96 | 0.51 | -3.22 | 2.63 | 1.64 |
| 6f | 3.28 | 1.98 | 0.50 | -3.28 | 2.7 | 1.65 |
| 6 g | 3.27 | 1.98 | 0.51 | -3.27 | 2.7 | 1.65 |
| 6h | 3.86 | 1.64 | 0.61 | -3.86 | 4.54 | 2.35 |
| 6i | 3.34 | 2.00 | 0.50 | -3.34 | 2.79 | 1.67 |
| 6j | 3.27 | 1.98 | 0.51 | -3.27 | 2.7 | 1.65 |

 η =chemical hardness; σ , chemical softness; ω , global electrophilicity; χ , electronegativity; μ , chemical potential; $\Delta Nmax=$ maximum electronic charge.

The electronic and global reactivity properties of the synthesized compounds provide crucial insights into their stability, reactivity, and potential for biological activity (Tables 7 and 8). These parameters include total energy (E), frontier molecular orbital energies ($E_{\mbox{\scriptsize HOMO}}$ and E_{LUMO}), ionization potential (I), electron affinity (A), energy gap (Eg), and dipole moment. Each of these factors plays a significant role in determining the chemical behavior and interaction potential of the molecules. The total energy (E), measured in atomic units (a.u.), represents the overall stability of a molecule, with more negative values indicating greater stability. Among the synthesized compounds, compound 6g exhibits the lowest total energy (-4302.00 a.u.), making it the most stable, while compound 6c has the highest total energy (-1720.21 a.u.), indicating comparatively lower stability. The frontier molecular orbitals, HOMO and LUMO, dictate the electron-donating and electronaccepting capabilities of the compounds. E_{HOMO} reflects the ability of a molecule to donate electrons, while E_{LUMO} indicates its ability to accept electrons. Among the studied compounds, compound 6h has the lowest E_{HOMO} value (-5.50 eV), making it the weakest electron donor, whereas compound 6d has the highest EHOMO value (-4.96 eV), suggesting that it is the most effective electron donor. Similarly, compound 6h also has the lowest E_{LUMO} value (-2.22 eV), making it the strongest electron acceptor, whereas compound 6d has the highest E_{LUMO} value (-1.14 eV), indicating weaker electron-accepting ability. These orbital energies play a vital role in determining molecular reactivity, as a lower energy gap between EHOMO and ELUMO signifies enhanced charge transfer potential. The ionization potential, which corresponds to the energy required to remove an electron from the molecule ($I = -E_{HOMO}$), is an essential indicator of molecular stability. Compound 6h exhibits the highest ionization potential (5.50 eV), meaning it strongly retains its electrons and is less likely to undergo oxidation, whereas compound 6d has the lowest ionization potential (4.96 eV), suggesting it more readily donates electrons. Similarly, electron affinity ($A = -E_{LUMO}$) measures the molecule's tendency to accept electrons. Compound 6h has the highest electron affinity (2.22 eV), making it the most likely to gain an electron, whereas compound 6d has the lowest electron affinity (1.14 eV), making it less receptive to additional electrons. These factors are crucial in defining the redox potential and interaction of the synthesized compounds with biological targets. A larger energy gap suggests greater stability but lower reactivity, whereas a smaller energy gap indicates higher chemical reactivity and enhanced charge transfer ability. Among the synthesized compounds, compound 6i has the highest energy gap (4.01 eV), indicating significant stability and lower chemical reactivity, while compound 6h has the lowest energy gap (3.28 eV), suggesting greater reactivity. This aligns with the high electron affinity and ionization potential of 6h, making it a more reactive compound compared to the others. Among the compounds, compound 6h exhibits the highest dipole moment (7.8696 D), indicating strong polarity and potential for increased bioavailability, whereas compound 6d has the lowest dipole moment (1.3451 D), and suggesting weaker interactions in polar environments. The dipole moment plays a crucial role in molecular recognition, binding affinity, and the overall pharmacological properties of

| Mode | Theoretical (scaled,cm ⁻¹) | Experimental (cm ⁻¹) | Assignments |
|------|--|----------------------------------|---|
| 171 | 3381 | 3355 | N-H stretch |
| 164 | 3080 | 3049 | sp ² C—H stretch of phenyl ring (Ring A) |
| 158 | 2981 | 2982 | sp ³ CH ₂ asymmetric stretch (C14-H ₂ , C15-H ₂ , C17-H ₂ , C18-H ₂) of morpholine ring (Ring E) |
| 154 | 2919 | 2865 | sp ³ CH ₂ symmetric stretch (C14-H ₂) of ring E and C12-H ₂ |
| 149 | 2877 | _ | sp ³ CH ₂ symmetric stretch (C15-H ₂) of morpholine |
| 145 | 1598 | 1638 | C = C stretch of thiazole ring (Ring D) |
| 144 | 1569 | 1597 | C = C stretch of ring D, $C = N$ stretches (C22=N26 and C22=N21) |
| 142 | 1528 | 1506 | C10=N11 stretch and C8=C9 stretch (thiosemicarbazone linkage and pyrazole ring) |
| 139 | 1486 | 1437 | C = C stretch of phenyl ring (Ring A) |
| 128 | 1404 | 1401 | C = C stretch of thiazole ring (Ring D) |
| 124 | 1350 | 1313 | sp³ CH₂ bending (ring E), sp³ CH₃ bending, and C8=N7 stretch |
| 115 | 1284 | _ | C30=C56 stretch |
| 105 | 1165 | 1173 | C-F stretch of CF₃ group |
| 97 | 1094 | 1110 | C—O stretch of C15-O16-C17 in morpholine ring |
| 92 | 1049 | 1067 | Ring D deformation |
| 83 | 991 | 1014 | H53-C28-C29-H52 twisting vibration |
| 75 | 892 | 921 | Ring A C—H out-of-plane bending |
| 69 | 814 | 846 | Ring D C—H out-of-plane bending |

Where, ring A- N-phenyl, ring B-pyrazole, ring C- thiazole, ring p- 4-trifluorophenyl, and ring E-morpholine.

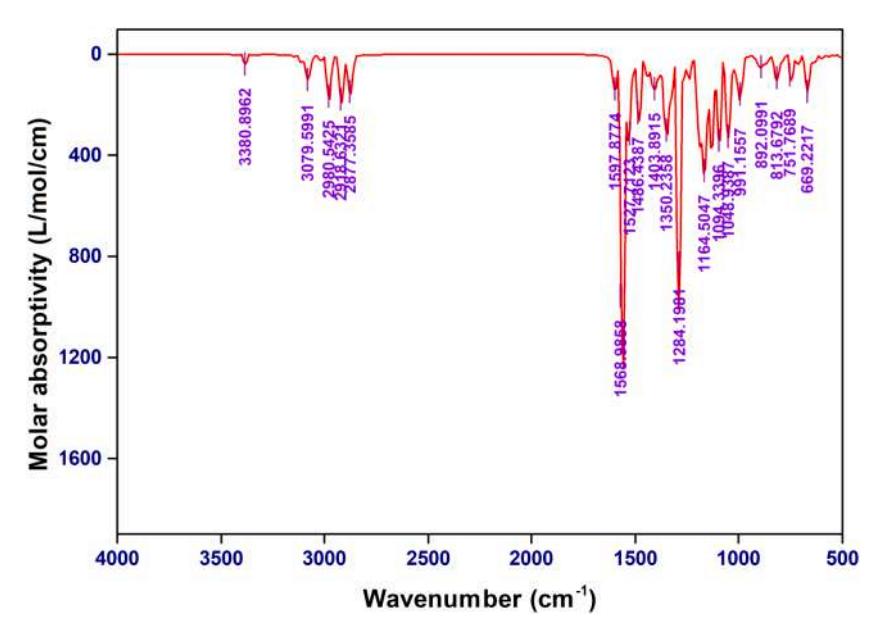


Fig. 7. Theoretical IR spectra of compound 6i.

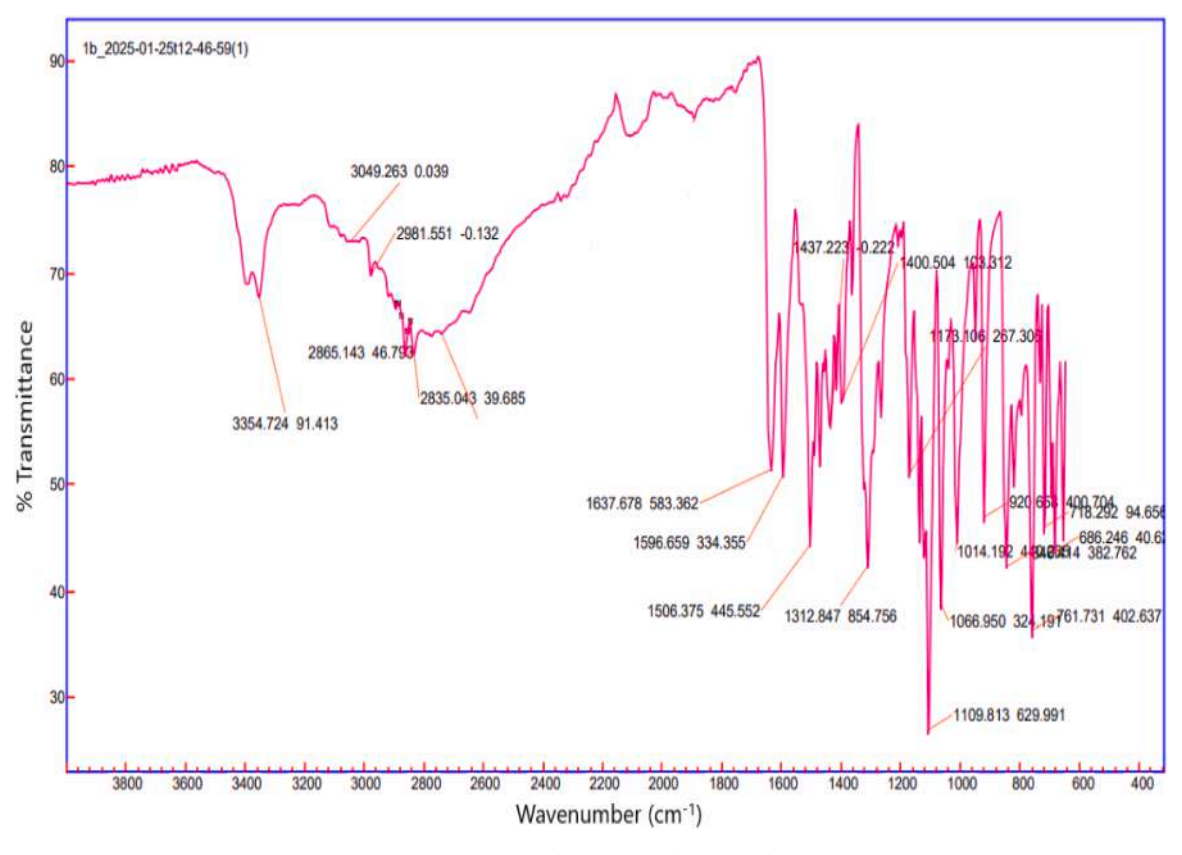


Fig. 8. Experimental IR spectra of compound 6i.

the chemical compounds.

The global reactivity parameters provide a comparative understanding of the chemical stability and reactivity of the synthesized compounds. Electronegativity (χ), which measures the ability to attract electrons, is highest for **6h** (3.86 eV), making it the strongest electron acceptor, while **6d** has the lowest χ (3.05 eV), indicating weaker electron-attracting ability. Correspondingly, chemical potential (μ), which represents the tendency of electrons to escape, follows the same trend, with **6h** having the highest μ (4.54 eV), making it the most

reactive, while **6d** has the lowest μ (2.44 eV), suggesting higher stability. Chemical hardness (η), which describes resistance to electron transfer, is highest for **6i** (2.00 eV), making it the most stable and least reactive, whereas **6h** has the lowest η (1.64 eV), indicating the highest reactivity. Chemical softness (σ), the inverse of hardness, shows that 4 h (0.61 eV⁻¹) is the softest and thus most reactive compound, while **6f** and **6i** (0.50 eV⁻¹) are the hardest and least reactive. Global electrophilicity (ω), a measure of a molecule's tendency to accept electrons, is highest for **6h** (-3.86 eV), reinforcing its strong electrophilic nature, while **6d** has the

lowest ω (-3.05 eV), making it the least electrophilic. Lastly, maximum electronic charge transfer (Δ Nmax), which indicates how much charge a molecule can accept, is highest for **6h** (2.35 eV), confirming its superior electron-accepting ability, while **6d** (1.60 eV) has the lowest, indicating limited charge transfer capacity. The **6h** emerges as the most reactive, electrophilic, and electron-attracting compound, while **6i** and **6d** are the most stable and least reactive.

3.5.5. Vibrational assignments study

The infrared spectra (IR) of Compound 6i were studied both experimentally and theoretically. The theoretical values were obtained using DFT method and B3LYP/6-31G(d,p) level of theory. To account for the overestimation of vibrational frequencies common in quantum chemistry computations, these theoretical values were scaled using the 0.96 scaling factor. For vibrational band assignments, the experimental infrared spectra were compared with the scaled theoretical wavenumbers (Table 9). The Figs. 7 and 8 represent theoretical and experimental IR spectra of compound 6i, respectively. The N-H stretching mode at 3381 cm⁻¹ (theoretical) corresponds well with the experimental band at 3355 cm⁻¹, confirming the presence of the hydrazine moiety. The sp² C-H stretching vibrations of the phenyl ring (Ring A) were observed at 3049 cm⁻¹, matching closely with the calculated value of 3080 cm⁻¹. The sp³ CH₂ asymmetric and symmetric stretching modes from the morpholine ring (Ring E) appeared at 2982 cm⁻¹ and 2865 cm⁻¹ ¹, respectively, in line with the theoretical predictions. The strong bands between 1400 and 1600 cm⁻¹ were attributed to C = N and C = Cstretching vibrations from the pyrazole, thiazole, and phenyl rings, confirming their structural integrity. The C-F stretching mode of the CF₃ group was detected at 1173 cm⁻¹, which aligns well with the theoretical value of 1165 cm⁻¹, and the C-O stretching vibration of morpholine at 1110 cm⁻¹ also matches the predicted value at 1094 cm⁻¹. The out-ofplane C-H bending modes for phenyl and trifluorophenyl rings were observed in the 800-900 cm⁻¹ region and are consistent with the theoretical data. Overall, the comparison between the theoretical and experimental spectra validates the molecular structure of compound 6i and confirms the presence of all expected functional groups. The good correlation between the scaled theoretical and experimental wavenumbers demonstrates the reliability of the DFT/B3LYP-6-31G(d,p) method in predicting vibrational frequencies, thus supporting the structural confirmation and experimental findings for the synthesized compound.

4. Conclusion

In this study, a series of pyrazole-thiazole derivatives was successfully synthesized and structurally characterized using advanced spectroscopic techniques. Among the synthesized compounds, 6i emerged as the most potent antitubercular agent with an MIC value of 12.5 µg/mL, attributed to the trifluoromethyl group's influence on enhancing lipophilicity and target binding. Molecular docking studies confirmed the strong binding of 6i to CYP51, emphasizing its potential as a CYP51 inhibitor. The extensive interaction profile of compound 6i, including hydrogen bonding, hydrophobic interactions, and π -stacking, suggests its ability to disrupt sterol biosynthesis in Mycobacterium tuberculosis. These findings provide valuable insights into the structure-activity relationship of pyrazole-thiazole hybrids and highlight compound 6i as a promising lead for further development. The integration of molecular docking and DFT analysis provided important insights into its binding affinity and electronic properties, while ADME profiling confirmed its favorable pharmacokinetics and drug-likeness. These findings underscore the potential of pyrazole-thiazole hybrids as valuable scaffolds in tuberculosis drug discovery, with compound 6i serving as a promising lead for further preclinical development. Future work will focus on optimizing its structure and evaluating its efficacy through comprehensive in vitro and in vivo studies.

CRediT authorship contribution statement

Yuvraj R. Sable: Writing – review & editing, Writing – original draft, Methodology, Investigation. Vishnu A. Adole: Writing – review & editing, Writing – original draft, Supervision, Software, Methodology, Investigation, Formal analysis, Conceptualization. Rahul A. Shinde: Writing – review & editing, Writing – original draft, Software. Hemant S. Deshmukh: Methodology, Investigation. R. Rajesh: Writing – original draft, Software, Investigation. Tahani Mazyad Almutairi: Writing – original draft, Software, Funding acquisition. Mahboob Alam: Writing – original draft, Resources. Mohammad Shahidul Islam: Writing – original draft, Validation, Funding acquisition.

Declaration of competing interest

The authors declare that they have no known competing financial interests or personal relationships that could have appeared to influence the work reported in this paper.

Acknowledgment

This work was funded by the Ongoing Research Funding program, (ORF-2025–1100), King Saud University, Riyadh, Saudi Arabia. The authors sincerely acknowledge CIF, Savitribai Phule Pune University, Pune, for NMR analysis of the synthesized compounds. Gratitude is extended to the Research Centre in Chemistry, Loknete Vyankatrao Hiray Arts, Science, and Commerce College, Panchavati, Nashik, and the Department of Chemistry for providing laboratory facilities. The authors also thank Maratha Mandal's Central Research Laboratory, Maratha Mandal's NGH Institute of Dental Sciences & Research Centre, Belgaum, Karnataka, for antitubercular screening.

Supplementary materials

Supplementary material associated with this article can be found, in the online version, at doi:10.1016/j.molstruc.2025.142891.

Data availability

Data will be made available on request.

References

- S. Perveen, D. Kumari, K. Singh, R. Sharma, Tuberculosis drug discovery: progression and future interventions in the wake of emerging resistance, Eur. J. Med. Chem. 229 (2022) 114066.
- [2] M. Mahmoud, Y. Tan, New advances in the treatments of drug-resistant tuberculosis, Expert. Rev. Anti. Infect. Ther. 21 (8) (2023) 863–870.
- [3] T. Umumararungu, M.J. Mukazayire, M. Mpenda, M.F. Mukanyangezi, J. B. Nkuranga, J. Mukiza, E.O. Olawode, A review of recent advances in anti-tubercular drug development, Indian J. Tuberc. 67 (4) (2020) 539–559.
- [4] E. Pontali, M.C. Raviglione, G.B. Migliori, Regimens to treat multidrug-resistant tuberculosis: past, present and future perspectives, Eur. Respir. Rev. 28 (152) (2019).
- [5] M. Mondoni, L. Saderi, G. Sotgiu, Novel treatments in multidrug-resistant tuberculosis, Curr. Opin. Pharmacol. 59 (2021) 103–115.
- [6] E. Kabir, M. Uzzaman, A review on biological and medicinal impact of heterocyclic compounds, Results. Chem. 4 (2022) 100606.
- [7] A. De, S. Sarkar, A. Majee, Recent advances on heterocyclic compounds with antiviral properties, Chem. Heterocycl. Compd. 57 (4) (2021) 410–416.
- [8] T. Qadir, A. Amin, P.K. Sharma, I. Jeelani, H. Abe, A review on medicinally important heterocyclic compounds, Open. Med. Chem. J. 16 (1) (2022).
- [9] K. Rajagopal, S. Dhandayutham, M. Nandhagopal, M. Narayanasamy, M. I. Elzagheid, L. Rhyman, P. Ramasami, Thiazole derivatives: synthesis, characterization, biological and DFT studies, J. Mol. Struct. 1255 (2022) 132374.
- [10] Y. Li, N. Sun, H.L. Ser, W. Long, Y. Li, C. Chen, B. Zheng, X. Huang, Z. Liu, Y.J. Lu, Antibacterial activity evaluation and mode of action study of novel thiazolequinolinium derivatives, RSC. Adv. 10 (25) (2020) 15000–15014.
- [11] F. Lemilemu, M. Bitew, T.B. Demissie, R. Eswaramoorthy, M. Endale, Synthesis, antibacterial and antioxidant activities of thiazole-based Schiff base derivatives: a combined experimental and computational study, BMC. Chem. 15 (1) (2021) 67.
- [12] R. Raveesha, A.M. Anusuya, A.V. Raghu, K.Y. Kumar, M.D. Kumar, S.B. Prasad, M. K. Prashanth, Synthesis and characterization of novel thiazole derivatives as

- potential anticancer agents: molecular docking and DFT studies, Comput. Toxicol. 21 (2022) 100202.
- [13] A.M. El-Naggar, A. Zidan, E.B. Elkaeed, M.S. Taghour, W.A. Badawi, Design, synthesis and docking studies of new hydrazinyl-thiazole derivatives as anticancer and antimicrobial agents, J. Saudi Chem. Soc. 26 (4) (2022) 101488.
- [14] T.A. Farghaly, A.M. Alsaedi, N.A. Alenazi, M.F. Harras, Anti-viral activity of thiazole derivatives: an updated patent review, Expert. Opin. Ther. Pat. 32 (7) (2022) 791–815.
- [15] E. Gürsoy, E.D. Dincel, L. Naesens, N.U. Güzeldemirci, Design and synthesis of novel Imidazo [2, 1-b] thiazole derivatives as potent antiviral and antimycobacterial agents, Bioorg. Chem. 95 (2020) 103496.
- [16] G.L. Khatik, A.K. Datusalia, W. Ahsan, P. Kaur, M. Vyas, A. Mittal, S.K. Nayak, A retrospect study on thiazole derivatives as the potential antidiabetic agents in drug discovery and developments, Curr. Drug Discov. Technol. 15 (3) (2018) 163–177.
- [17] T. Kalita, A. Choudhury, A. Shakya, S.K. Ghosh, U.P. Singh, H.R. Bhat, A review on synthetic thiazole derivatives as an antimalarial agent, Curr. Drug Discov. Technol. 21 (5) (2024) 10–42.
- [18] Z. Zhang, P. Cao, M. Fang, T. Zou, J. Han, Y. Duan, H. Xu, X. Yang, Q.S. Li, Design, synthesis, and SAR study of novel 4, 5-dihydropyrazole-thiazole derivatives with anti-inflammatory activities for the treatment of sepsis, Eur. J. Med. Chem. 225 (2021) 113743.
- [19] G. Kumar, N.P. Singh, Synthesis, anti-inflammatory and analgesic evaluation of thiazole/oxazole substituted benzothiazole derivatives, Bioorg. Chem. 107 (2021) 104608.
- [20] M.S. Shah, M.M. Rahman, M.D. Islam, A. Al-Macktuf, J.U. Ahmed, H. Nishino, M. A. Haque, Synthesis, antimicrobial and antioxidant evaluation with in silico studies of new thiazole Schiff base derivatives, J. Mol. Struct. 1248 (2022) 131465.
- [21] R. Raveesha, K.Y. Kumar, M.S. Raghu, S.B. Prasad, A. Alsalme, P. Krishnaiah, M. K. Prashanth, Synthesis, molecular docking, antimicrobial, antioxidant and anticonvulsant assessment of novel S and C-linker thiazole derivatives, Chem. Phys. Lett. 791 (2022) 139408.
- [22] I. Saleh, H.R. Kc, S. Roy, M.K. Abugazleh, H. Ali, D. Gilmore, M.A. Alam, Design, synthesis, and antibacterial activity of N-(trifluoromethyl) phenyl substituted pyrazole derivatives, RSC. Med. Chem. 12 (10) (2021) 1690–1697.
- [23] N.A. Alshaye, N.S. Alharbi, M.A. El-Atawy, R.O. El-Zawawy, E.A. Hamed, M. Elhag, H.A. Ahmed, A.Z. Omar, Synthesis, DFT, and in silico biological evaluation of chalcone bearing pyrazoline ring against Helicobacter pylori receptors, Heliyon 10 (14) (2024).
- [24] M.A. El-Atawy, R. Kebeish, A.R.Z. Almotairy, A.Z. Omar, Design, synthesis, characterization, and cytotoxicity of new pyrazolylmethylene-2thioxoimidazolidin-4-one derivatives towards androgen-sensitive LNCaP prostate cancer cells, Biomolecules 14 (7) (2024) 811.
- [25] H.E. Abdelwahab, H.Z. Ibrahim, A.Z. Omar, Design, synthesis, DFT, molecular docking, and biological evalution of pyrazole derivatives as potent acetyl cholinestrease inhibitors, J. Mol. Struct. 1271 (2023) 134137.
- [26] Z. Liang, Z. Rong, H. Cong, D. Qing-Ying, S. Ming-Zhu, W. Jie, N. Xu-Liang, C. Jin-Zhu, C. Shang-Xing, P. Da-Yong, Design, synthesis and antifungal activity of novel pyrazole amides derivates. J. Mol. Struct. 1277 (2023) 134881.
- pyrazole amides derivates, J. Mol. Struct. 1277 (2023) 134881.

 [27] A.A. Bekhit, S.N. Nasralla, E.J. El-Agroudy, N. Hamouda, A. Abd El-Fattah, S. A. Bekhit, K. Amagase, T.M. Ibrahim, Investigation of the anti-inflammatory and analgesic activities of promising pyrazole derivative, Eur. J. Pharm. Sci. 168 (2022) 106080
- [28] K. Kumara, M.G. Prabhudeva, C.B. Vagish, H.K. Vivek, K.M.L. Rai, N.K. Lokanath, K.A. Kumar, Design, synthesis, characterization, and antioxidant activity studies of novel thienyl-pyrazoles, Heliyon 7 (7) (2021).
- [29] E.K. Abdelall, G.M. Kamel, Synthesis of new thiazolo-celecoxib analogues as dual cyclooxygenase-2/15-lipoxygenase inhibitors: determination of regio-specific different pyrazole cyclization by 2D NMR, Eur. J. Med. Chem. 118 (2016) 250-258
- [30] J. Yuan, C. Yuan, A. Degterev, Unsaturated heterocyclic inhibitors of necroptosis, PCT Int. Appl.—2010.—WO (2010) 2010075290.
- [31] D.G. Raut, A.S. Lawand, V.D. Kadu, M.G. Hublikar, S.B. Patil, D.G. Bhosale, R. B. Bhosale, Synthesis of asymmetric thiazolyl pyrazolines as a potential antioxidant and anti-inflammatory agents, Polycycl. Aromat. Compd. 42 (1) (2021) 70–79.
- [32] P. Khloya, S. Kumar, P. Kaushik, P. Surain, D. Kaushik, P.K. Sharma, Synthesis and biological evaluation of pyrazolylthiazole carboxylic acids as potent antiinflammatory-antimicrobial agents, Bioorg. Med. Chem. Lett. 25 (6) (2015) 1177–1181.
- [33] K. Veena, M.S. Raghu, K.Y. Kumar, C.P. Kumar, F.A. Alharti, M.K. Prashanth, B. H. Jeon, Design and synthesis of novel benzimidazole linked thiazole derivatives as promising inhibitors of drug-resistant tuberculosis, J. Mol. Struct. 1269 (2022) 133822.
- [34] L.H.B. Maganti, D. Ramesh, B.G. Vijayakumar, M.I.K. Khan, A. Dhayalan, J. Kamalraja, T. Kannan, Acetylene containing 2-(2-hydrazinyl) thiazole derivatives: design, synthesis, and in vitro and in silico evaluation of antimycobacterial activity against mycobacterium tuberculosis, RSC. Adv. 12 (14) (2022) 8771–8782.
- [35] M.M. Shaaban, M. Teleb, H.M. Ragab, M. Singh, B.H. Elwakil, L.A. Heikal, D. Sriram, M.A. Mahran, The first-in-class pyrazole-based dual InhA-VEGFR inhibitors towards integrated antitubercular host-directed therapy, Bioorg. Chem. 145 (2024) 107179.
- [36] A. Kumari, R.K. Singh, Morpholine: pharmacophore modulating pharmacokinetic properties of anticancer leads. Key Heterocyclic Cores For Smart Anticancer Drug-Design Part II, 2022, pp. 137–173.

- [37] H.S. Deshmukh, V.A. Adole, A. Kumar, N. Misra, S.D. Pawar, S.R. Tambe, B. S. Jagdale, Synthesis, spectroscopic (IR and NMR), HOMO-LUMO, NLO, molecular docking and ADME study of (E)-2-(2-((5-chloro-3-methyl-1-phenyl-1H-pyrazol-4-yl) methylene) hydrazineyl)-4-(4-nitrophenyl) thiazole, J. Mol. Struct. 1305 (2024) 137745.
- [38] K.B. Gangurde, R.A. More, V.A. Adole, D.S. Ghotekar, Design, synthesis and biological evaluation of new series of benzotriazole-pyrazole clubbed thiazole hybrids as bioactive heterocycles: antibacterial, antifungal, antioxidant, cytotoxicity study, J. Mol. Struct. 1299 (2024) 136760.
- [39] K.B. Gangurde, R.A. More, V.A. Adole, D.S. Ghotekar, Synthesis, antibacterial, antifungal, antioxidant, cytotoxicity and molecular docking studies of thiazole derivatives, Results. Chem. 7 (2024) 101380.
- [40] Y.R. Sable, V.A. Adole, E.A. Pithawala, R.D. Amrutkar, Design, synthesis, and antitubercular evaluation of piperazinyl-pyrazolyl-2- hydrazinyl thiazole derivatives: experimental, DFT and molecular docking insights, J. Sulfur Chem. (2025) 1–26.
- [41] S. El Rhabori, A. El Aissouq, O. Daoui, S. Elkhattabi, S. Chtita, F. Khalil, Design of new molecules against cervical cancer using DFT, theoretical spectroscopy, 2D/3D-QSAR, molecular docking, pharmacophore and ADMET investigations, Heliyon 10 (3) (2024).
- [42] V.A. Adole, S.S. Shinde, R. Nikam, R.K. More, A.R. Kumar, S. Selvaraj, S.N. Mali, S. K. Ghotekar, Y. Sarnikar, S. Mahurkar, Synthesis, antibacterial, antifungal, antioxidant, DFT, molecular docking, and ADME study of two new thiazole-based derivatives featuring nitrophenyl and benzonitrile functionalities, J. Mol. Struct. (2025) 141305.
- [43] F. Stanzione, I. Giangreco, J.C. Cole, Use of molecular docking computational tools in drug discovery, Prog. Med. Chem. 60 (2021) 273–343.
- [44] V.A. Adole, A. Kumar, N. Misra, R.A. Shinde, B.S. Jagdale, Synthesis, computational, antimicrobial, antioxidant, and ADME study of 2-(3, 4-dimethoxyphenyl)-4 H-chromen-4-one, Polycycl. Aromat. Compd. 44 (8) (2024) 5397–5411.
- [45] K.B. Gangurde, V.A. Adole, D.S. Ghotekar, Computational study: synthesis, spectroscopic (UV–vis, IR, NMR), antibacterial, antifungal, antioxidant, molecular docking and ADME of new (E)-5-(1-(2-(4-(2, 4-dichlorophenyl) thiazol-2-yl) hydrazineylidene) ethyl)-2, 4-dimethylthiazole, Results. Chem. 6 (2023) 101093.
- [46] V.A. Adole, Computational chemistry approach for the investigation of structural, electronic, chemical and quantum chemical facets of twelve Biginelli adducts, Organomet. Chem. 1 (1) (2021) 29–40.
- [47] M.J. Frish, G.W. Trucks, H.B. Schlegel, G.E. Scuseria, M.A. Robb, J.R. Cheeseman, V.G. Zakrzevski, J.A. Montgomery Jr, T. Vreven, K.N. Kudin, J.C. Burant, Gaussian 03, Revision C. 02, Gaussian. Inc., Wallingford, CT, 2004.
- [48] A.D. Becke, Density-functional thermochemistry. III. The role of exact exchange, J. Chem. Phys. 98 (7) (1993) 5648–5652.
- [49] C. Lee, W. Yang, R.G. Parr, Development of the Colle-Salvetti correlation-energy formula into a functional of the electron density, Phys. Rev. B 37 (2) (1988) 785.
- [50] R.D.I.I. Dennington, Todd Keith, John Millam, GaussView, version 4.1. 2, Semichem Inc. Shawnee Mission KS (2007).
- [51] A. Daina, O. Michielin, V. Zoete, SwissADME: a free web tool to evaluate pharmacokinetics, drug-likeness and medicinal chemistry friendliness of small molecules, Sci. Rep. 7 (1) (2017) 42717.
 [52] M.C. Lourenco, M.V. de Souza, A.C. Pinheiro, M.D.L. Ferreira, R.S. Gonçalves, T.C.
- [52] M.C. Lourenco, M.V. de Souza, A.C. Pinheiro, M.D.L. Ferreira, R.S. Gonçalves, T.C. M. Nogueira, M.A. Peralta, Evaluation of anti-tubercular activity of nicotinic and isoniazid analogues, ARKIVOC. 15 (2007) 181–191.
- [53] O. Trott, A.J. Olson, AutoDock Vina: improving the speed and accuracy of docking with a new scoring function, efficient optimization, and multithreading, J. Comput. Chem. 31 (2) (2010) 455–461.
- [54] M.B. Alhawarri, Exploring the anticancer potential of Furanpydone A: a computational study on its inhibition of MTHFD2 across diverse cancer cell lines, Cell Biochem, Biophys (2024) 1–18.
- [55] D.A.E. Pitaloka, D.S.F. Ramadhan, Arfan, L. Chaidir, T.M. Fakih, Docking-based virtual screening and molecular dynamics simulations of quercetin analogs as enoyl-acyl carrier protein reductase (InhA) inhibitors of mycobacterium tuberculosis. Sci. Pharm. 89 (2) (2021) 20.
- [56] A. Hantzsch, J.H. Weber, Ueber verbindungen des thiazols (pyridins der thiophenreihe), Ber. Dtsch. Chem. Ges. 20 (2) (1887) 3118–3132.
- [57] D.X. Duc, N.T. Chung, Recent development in the synthesis of thiazoles, Curr. Org. Synth. 19 (6) (2022) 702–730.
- [58] V.A. Adole, R.A. More, B.S. Jagdale, T.B. Pawar, S.S. Chobe, Efficient synthesis, antibacterial, antifungal, antioxidant and cytotoxicity study of 2-(2-hydrazineyl) thiazole derivatives, ChemistrySelect. 5 (9) (2020) 2778–2786.
- [59] Silverstein, R.M. and Webster, F.X., Spectrometric Identification of Organic Compounds. New York: Wiley.
- [60] Pavia, D.L., Lampman, G.M. and Kriz, G.S., Introduction to Spectroscopy. Boston: Cengage Learning.
- [61] G.I. Lepesheva, M.R. Waterman, Sterol 14α-demethylase cytochrome P450 (CYP51), a P450 in all biological kingdoms, Biochim. Biophys. Acta (BBA)-Gen. Subj. 1770 (3) (2007) 467–477.
- [62] K.J. McLean, A.J. Dunford, R. Neeli, M.D. Driscoll, A.W. Munro, Structure, function and drug targeting in mycobacterium tuberculosis cytochrome P450 systems, Arch. Biochem. Biophys. 464 (2) (2007) 228–240.
- [63] A. Campaniço, R. Moreira, F. Lopes, Drug discovery in tuberculosis. New drug targets and antimycobacterial agents, Eur. J. Med. Chem. 150 (2018) 525–545.
- [64] A. Saral, P. Sudha, S. Muthu, S. Sevvanthi, A. Irfan, Molecular structure spectroscopic elucidation, IEFPCM solvation (UV–Vis, MEP, FMO, NBO, NLO), molecular docking and biological assessment studies of lepidine (4-Methylquinoline), J. Mol. Liq. 345 (2022) 118249.

- [65] H.A. Hussein, A DFT study of structural-stability, Mulliken charges, MEP, FMO, and NLO properties of trans alkenyl substituted chalcones conformers: theoretical study, Struct. Chem. 34 (6) (2023) 2201–2223.
- [66] S. Selvaraj, In silico studies on the molecular geometry, FMO, mulliken charges, MESP, ADME and molecular docking prediction of pyrogallol carboxaldehydes as potential anti-tumour agents, Phys. Chem. Res. 12 (2) (2024) 305–320.
- [67] R. Satheeshkumar, K. Prabha, K.N. Vennila, K. Sayin, E. Güney, W. Kaminsky, R. Acevedo, Spectroscopic (FT-IR, NMR, single crystal XRD) and DFT studies including FMO, Mulliken charges, and Hirshfeld surface analysis, molecular docking and ADME analyses of 2-amino-4'-fluorobenzophenone (FAB), J. Mol. Struct. 1267 (2022) 133552.
- [68] R.H. Waghchaure, V.A. Adole, DFT computational studies, spectroscopic (UV–Vis, IR, NMR), in silico molecular docking and ADME study of 3-(3-methylpyridin-2-yl)-5-phenyl-1, 2, 4-oxadiazole, J. Mol. Struct. 1296 (2024) 136724.
- [69] K. Srishailam, L. Ravindranath, B. Venkatram Reddy, G. Ramana Rao, Electronic spectra (experimental and simulated), and DFT investigation of NLO, FMO, NBO, and MESP characteristics of some biphenylcarboxaldehydes, Polycycl. Aromat. Compd. 43 (8) (2023) 7200–7213.
- [70] H.S. Deshmukh, V.A. Adole, S.B. Wagh, V.M. Khedkar, B.S. Jagdale, Exploring N-heterocyclic linked novel hybrid chalcone derivatives: synthesis, characterization, evaluation of antidepressant activity, toxicity assessment, molecular docking, DFT and ADME study, RSC. Adv. 15 (20) (2025) 16187–16210.
- [71] S.S. Pathade, B.S. Jagdale, Experimental and computational investigations on the molecular structure, vibrational spectra, electronic properties, FMO and mep analyses of 4, 6-bis (4-Fluorophenyl)-5, 6-dihydropyrimidin-2 (1H)-one: a DFT insight, Phys. Chem. Res. 8 (4) (2020) 671–687.